

UC Merced

UC Merced Electronic Theses and Dissertations

Title

Stable Isotopes and Late Quaternary Environments: A Woodrats' Tale

Permalink

<https://escholarship.org/uc/item/0tz85567>

Author

Shaver, Constance

Publication Date

2022

Peer reviewed|Thesis/dissertation

UNIVERSITY OF CALIFORNIA, MERCED

Stable Isotopes and Late Quaternary Environments: A Woodrats' Tale

A Thesis submitted in partial satisfaction of the requirements
for the degree of Master of Science

in

Environmental Systems

by

Constance Matthiessen Shaver

Committee in charge:

Professor Jessica Blois, Advisor & Degree Committee Chair

Professor Sora Kim, Examination Chair

Professor Rebecca Ryals

Robin Trayler

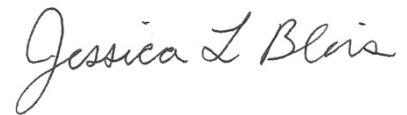
2022

Copyright

Constance Shaver, 2022

All rights reserved

The Thesis of Constance Shaver is approved, and it is acceptable in quality and form for publication on microfilm and electronically:



Dr. Jessica Blois, Advisor



Dr. Sora Kim, Chair



Dr. Rebecca Ryals



Dr. Robin Trayler

University of California, Merced

2022

Table of Contents

| | |
|---|------|
| List of Tables..... | v |
| List of Figures..... | vi |
| Acknowledgments..... | vii |
| Abstract..... | viii |
| Introduction..... | 1 |
| Paleoclimate in Northern California..... | 2 |
| Neotoma fossils..... | 3 |
| Stable isotopes..... | 3 |
| Methods..... | 5 |
| Study systems..... | 5 |
| Chronology of cave deposits..... | 5 |
| Stable isotope analysis..... | 6 |
| Statistical analysis: Variation in SCPD stable isotope values through time..... | 7 |
| Statistical analysis: Correspondence between SCPD and other proxies..... | 7 |
| Results..... | 8 |
| Radiocarbon dates & chronology..... | 8 |
| Variation in stable isotopes values through time..... | 9 |
| Correspondence among SCPD and other paleoenvironmental proxies..... | 9 |
| Discussion..... | 10 |
| Change in carbon isotope values through time..... | 10 |
| Change in oxygen isotope values through time..... | 11 |
| SCCUT..... | 13 |
| Conclusions..... | 13 |
| Tables and Figures..... | 14 |
| Supplemental Tables and Figures..... | 21 |
| Literature Cited..... | 28 |

LIST OF TABLES

Table 1. Stable isotope values from the SCPD deposit by level

Table 2. The relationship between carbon and oxygen isotope values at SCPD and other proxies

LIST OF FIGURES

Figure 1. Location of Samwell Cave

Figure 2. Conceptual diagram showing overview of the isotopic study system

Figure 3. The updated SCPD age model

Figure 4. SCPD stable isotope values by level and age

Figure 5. SCPD stable isotope data compared with global and regional climate proxies

ACKNOWLEDGMENTS

The work presented in this thesis is the cumulation of many pivots, adjustments, and creative alternatives that would not have been possible without the support and contribution of my peers, mentors, and family.

Extra special thanks to my advisor Jessica Blois for always being supportive, patient, and my biggest advocate in all aspects of graduate school. I feel incredibly lucky to have learned from and worked alongside someone so smart and compassionate. I also thank my committee members: Sora Kim, Robin Trayler, and Rebecca Ryals for their suggestions and flexibility in what was a rather tight thesis turnaround. Thank you to my fun loving cohort for helping each other navigate the perils of starting graduate school during a global pandemic.

And of course, endless thanks to my biggest fans. My partner Lawrence Combs for reminding me I am smart when doubt crept in and our pooch Pablo who kept me smiling and adventuring throughout it all. My mom and dad (Molly and Marvin) for teaching me to always stay curious, and my big sister Ella who has never wavered in having my back and guiding me forward.

Finally, thank you to everyone throughout my life who ignored me when I said I wasn't any good at math or science.

This work was supported by NSF EAR 1750597 to Jessica L. Blois

ABSTRACT

Stable Isotopes and Late Quaternary Environments: A Woodrats Tale

Constance Matthiessen Shaver

Master of Science in Environmental Systems

University of California, Merced 2022

Advisor: Jessica Blois

Earth's environment has continuously changed throughout geologic history and species have been able to persist, evolve, or at times go extinct in response to those changes. However, while we have a baseline understanding of how climates have fluctuated through time and overall biodiversity responses to those fluctuations, we often lack a detailed understanding of those changes at the local scale. Small mammals are valuable recorders of environmental conditions, tracking changes that are more spatially sensitive than large mammals due to their small home ranges. This research explores isotopic patterns from small mammals (*Neotoma* spp.) as potential indicators of late Quaternary environmental conditions, by determining $\delta^{13}\text{C}$ and $\delta^{18}\text{O}$ values and comparing inferred isotope changes with known climatic, environmental, and ecological change in this region over the last 22 kya. Overall, our data show that the tooth enamel isotopes from *Neotoma* track global changes in carbon and oxygen associated with the transition from glacial to interglacial cycles but interpreting our data relative to local scale and temporally dynamic environmental changes is more challenging and could benefit from additional research.

INTRODUCTION

Earth's environment has continuously changed throughout geologic history and species have been able to persist, evolve, or at times go extinct in response to those changes (Crowley, 1983). At times, during very large climatic events in conjunction with other factors, the Earth experienced mass extinction events that resulted in enormous loss of biodiversity across the globe (McElwain & Punyasena, 2007; Twitchett, 2006). This is concerning because the rate and magnitude of anthropogenic climate change is increasing (Quintero & Wiens, 2013), causing substantial challenges to biological populations around the world and possibly leading to a 6th mass extinction event (Barnosky et al., 2011). Apart from mass extinctions, climate change has a number of other societally-relevant impacts on biodiversity (Barnosky et al., 2012; Bellard et al., 2012). Thus, it is imperative that we begin to understand the degree to which species were influenced by past climate and how (or if) they were able to respond in order to improve our understanding of how to preserve contemporary biodiversity in the face of anthropogenic climate changes.

The Quaternary, or the last ~2.5 million years [encompassing both the Pleistocene (2.58 Ma to 11.7 thousand years ago (kya) and the Holocene (11.7 kya to present)], is a particularly valuable time for studying climate change. The Earth experienced a series of dramatic shifts in temperature and moisture due to alternating glacial and interglacial regimes (Pisias & Moore, 1981). The most recent period of transition occurred during the late Quaternary following the Last Glacial Maximum (LGM) 22 kya as the northern hemisphere ice sheets retreated and the ecosystems comprised of the fauna and flora occurring today were established (Clark et al., 2009). Further, the late Quaternary also experienced highly variable climates between 15 – 11 kya with rapid warming at the start of the Bølling-Allerød, followed by rapid cooling during the Younger Dryas and another period of rapid warming at the end of the Younger Dryas during the transition from the Pleistocene to the early Holocene (Clark et al., 2012; Steffensen et al., 2008). Climate change across the late Quaternary also greatly impacted biodiversity, contributing to megafaunal extinctions (Barnosky et al., 2004). Even species that survived throughout the late Quaternary were impacted by climate: vegetation, for example, underwent major transformations over the last 21,000 years (Gill et al., 2009; Williams et al., 2004) and surviving small mammal species saw abundance and diversity changes (Blois et al., 2010). This time period thus provides a meaningful study system for understanding the effects of shifts in climate can have on biodiversity.

While we have a baseline understanding of how climates fluctuated through time and the overall biodiversity responses to those fluctuations, we often lack a detailed understanding of those changes at the local scale. Species have complex and individualistic relationships with their environments (e.g., Burbrink et al., 2016; Matias et al., 2017; Stralberg et al., 2009), and our interpretation of past environments can be difficult to infer from limited and often conflicting proxy data. Thus, assembling data from multiple proxies can improve our understanding of both past environmental changes and ecological responses to those changes (e.g., Birks & Birks, 2006; Davidson et al., 2013; Jones & Desantis, 2017).

In this thesis, I explore the use of stable isotope data from small mammals as potential indicators of late Quaternary environmental conditions, using $\delta^{13}\text{C}$ and $\delta^{18}\text{O}$

values and comparing inferred isotope changes with known climatic, environmental, and ecological change in this region over the last 22 kya. To do this, I focus on data from one taxon that survived the late Quaternary megafaunal extinctions (*Neotoma* spp.) at one site in northern California, Samwell Cave (Figure 1). I first provide an overview of paleoclimate in northern California across the late Quaternary, then review why stable isotopic data from *Neotoma* may provide a valuable proxy to better understand both past climate change and species response to those changes. Specifically, I investigate the following questions: 1) Have oxygen and carbon isotope values of *Neotoma* changed through time? and 2) Is paleoclimate inferred from Samwell Cave *Neotoma* fossils consistent with other regional proxies?

PALEOCLIMATE IN NORTHERN CALIFORNIA

A variety of global and regional proxies including ice cores, sediment cores, fossil pollen, and speleothems provide data to interpret paleoclimate in Northern California. The North Greenland Ice Core Project (NGRIP) contributes high resolution inferences of climate using oxygen isotopes (North Greenland Ice Core Project members, 2004). This dataset extends back approximately 250 kya and captures multiple episodes of abrupt climate change during the last glacial period (Dansgaard et al., 1993). Since $\delta^{18}\text{O}_{\text{NGRIP}}$ data is directly correlated to air temperature, this has been established as a global proxy for tracking large-scale environmental change with fine temporal resolution. The NGRIP record shows that global climate was cold and dry at the LGM (20 kya) and then transitioned rapidly during the Bølling-Allerød and Younger Dryas periods (15 – 11 kya) with a 28°C difference across 5,000 years (Platt et al., 2017). Temperatures increased again around 11 kya and have remained high throughout the Holocene to the present.

Sediment cores provide access to fossil pollen, which is a valuable proxy for tracking regional paleoenvironmental change and is most commonly applied to studies about paleovegetation and fire history (e.g., Daniels et al., 2005; Scott Anderson et al., 2008). Through the analysis of paleovegetation, fossil pollen also provides information about environmental conditions such as temperature and precipitation (Mohr et al., 2000) and can track climate controls that may have impacted vegetation over at least the last 100 kya (Whitlock & Bartlein, 1997). In Northern California, postglacial vegetation inferred from fossil pollen records indicate a subalpine parkland habitat between 16-13 kya, a shift to a pine and fir forest for 2 kya before experiencing a subsequent shift that resulted in a pine, oak, and conifer forest between 11-5 kya; the present-day region is now dominated by pine and fir trees (Mohr et al., 2000). Multiple paleovegetation studies in this region have provided data for paleoclimate reconstructions that show a cold and dry environment between 16-11 kya which then transitioned into warm and dry conditions until about 3kya when most sites experienced a shift to cooler and moister climates (Daniels et al., 2005).

Speleothem records provide useful regional proxies for understanding precipitation, aridity, and seasonality: isotope compositions of carbonate from the speleothem as well as the oxygen and hydrogen isotope values from the resulting drip water closely reflect precipitation events (Baker et al., 2019). Speleothems from two caves in California (Figure 1), Moaning Caverns (MC) and Lake Shasta Caverns (LSC), have been analyzed for their oxygen isotope composition which provides insights into regional paleoclimate. The MC dataset suggests warmer and drier conditions in central

California from 16.5 – 10.6 kya, while the LSC dataset to the north indicate drier conditions during the LGM with an increase in rainfall from about 18 – 14 kya (Oster et al., 2009, 2020).

NEOTOMA FOSSILS

One potential source of valuable paleoclimatic and paleoenvironmental information is small mammals since there is a relatively comprehensive fossil record of small mammals from the late Quaternary (FAUNMAP Working Group, 1994; Graham et al., 1996). Most of these fossils were deposited as pellets from various owls and other raptors who eat small mammals and other vertebrates. These predators are unable to digest teeth and bones from their prey, and thus excrete well-preserved bones and other hard parts in their pellets (Avenant, 2006). Woodrats (*Neotoma* spp.) sometimes transport these pellets to their middens, and if the middens occur in cave environments, the pellets and other midden materials can be well preserved in cave sediments (Andrews, 1990; Simms, 1994). Due to the link between woodrat middens and small mammal fossilization, one of the most well-represented taxa is *Neotoma*. *Neotoma* is also a useful focal species because it is extant, so inferences from past populations can be directly compared to modern populations. Furthermore, *Neotoma* spp. are herbivore generalists with small home ranges, typically foraging within a 500ft radius of their den. (Carraway & Verts, 1991), This implies the food they consume is sourced from a localized area and their isotopic signals reflect an indiscriminate sampling of available vegetation within their home range. However, there is very little research about the stable isotope signals recorded in modern small mammals, including *Neotoma*, and even less so for ancient communities (but see Tomé et al., 2021; Fox et al., in review).

STABLE ISOTOPES

Stable isotope analysis (SIA) is a well-established technique for interpreting past temperature, precipitation, and atmospheric CO₂ (Koch, 1998). Stable isotopes are also used in studies of mammal diet, water use, and migration through time (Clementz, 2012; Terry, 2018). Stable isotope analysis is frequently applied to mammalian bone and teeth – carbon ($\delta^{13}\text{C}$) and oxygen ($\delta^{18}\text{O}$) can be extracted from the tooth enamel whereas the organic component of dentin contains nitrogen ($\delta^{15}\text{N}$), which is often used to determine trophic level (Hedges & Reynard, 2007; Kelly, 2000). Previous research using SIA to reconstruct paleoenvironments has relied heavily on large mammals and generally excluded small mammals due to the difficulty of conducting destructive analysis on samples that size. However, rodent tooth enamel is particularly resilient to chemical alteration during fossilization and therefore maintains the original isotopic signal established during formation, as opposed to collagen which is more susceptible to breakdown (Sponheimer & Lee-Thorp, 1999). Additionally, $\delta^{13}\text{C}$ values from collagen records dietary protein, whereas enamel carbonate $\delta^{13}\text{C}$ values represents bulk diet (carbohydrates, lipids, protein) and therefore provides a more holistic interpretation of food consumption that is especially useful when studying herbivore generalists (Koch et al., 1997).

CARBON ($\delta^{13}\text{C}$)

Stable carbon isotopes are most commonly used to investigate paleovegetation and paleodiet of mammals since it is derived from consumed plant material. Most plants use one of two photosynthetic pathways (C_3 vs C_4 photosynthesis), and each one imparts a distinct range of $\delta^{13}\text{C}$ values that gets incorporated into the rodent's teeth after consumption. C_3 vegetation ranges between -32‰ to -19‰ with a mean value of -29‰ and the range for C_4 vegetation is -19‰ to -10‰ with a mean value of -14‰ (O'Leary, 1988). This range difference comes from the degree to which each pathway discriminates against the heavier isotope ^{13}C during fixation of CO_2 for photosynthesis. The large distribution in $\delta^{13}\text{C}$ values for C_3 is due to local environmental conditions that influence fractionation, such as temperature, water availability, and light conditions (Jeffrey et al., 2015). C_3 plants that inhabit shaded, subcanopy, humid environments will have low $\delta^{13}\text{C}$ values, whereas plants in arid, open environments will have higher $\delta^{13}\text{C}$ values that more closely resemble C_4 values (up to -21‰) (Gehler et al., 2012; Kohn, 2010). Since these variations are reflected in the teeth of rodents feeding in these environments, researchers can investigate changes in habitat-use, resource partitioning, and dietary preferences (Terry, 2018).

C_3 plants are more abundant globally, making up a majority of plants on earth, whereas C_4 plants are believed to be younger in origin and are less abundant (Cerling et al., 1993). The younger C_4 photosynthesis pathway originated as an adaptation to warmer and drier climates and C_4 plants have shown a strong resilience to aridity and high temperatures (Caemmerer et al., 2014). The different range in values of each pathway means that a shift seen in the $\delta^{13}\text{C}$ values of consumers could represent a climatic shift, given the environments in which each set of plants is able to succeed (or also possibly a dietary switch to consumption of different plants). C_3 plants are typically trees, shrubs, and bushes whereas C_4 are often grasses. Since *Neotoma* are non-discriminate generalists, a change in diet would record vegetation shifts and potentially signify a warming climate or transition to drier conditions, or both.

OXYGEN ($\delta^{18}\text{O}$)

Oxygen isotopes are commonly used to reconstruct precipitation, aridity, and paleotemperature within a region (Sponheimer & Lee-Thorp, 1999). Since mammals are endothermic, and therefore body temperature is constant and not impacted by environment, their $\delta^{18}\text{O}$ values are likely record environmental water oxygen isotope compositions rather than air temperature, though several studies have been able to account for the water-tissue fractionation factors and make direct comparisons (Podlesak et al., 2008; Peneycad et al., 2019). The $\delta^{18}\text{O}$ values of body water from mammals reflects oxygen inputs (i.e., drinking water, food water, respired oxygen) and oxygen outputs (i.e., respiration, fluids such as sweat, urine, feces) (Kohn 1996). In rodents, like other mammals, this affects the oxygen isotope composition from rodent teeth (Gehler et al., 2012). While many mammals are obligate drinkers and obtain much of their oxygen from drinking surface water, *Neotoma* are non-obligate drinkers and derive their water from food consumption, making the direct comparison to drinking water and environment more complicated though still feasible (Fernández-García et al., 2019; Jeffrey et al., 2015; Royer et al., 2013).

Plant water is usually enriched in the heavier oxygen isotope (^{18}O) relative to local meteoric water. This enrichment is due to the preferential transpiration of the lighter

isotope (^{16}O) from the plant surface which results in a remaining pool that is depleted of the lighter molecule and enriched with the heavy molecule. Evapotranspiration is temperature and moisture dependent and will therefore be enhanced with aridity and warmer conditions (Fernández-García et al., 2019; Gehler et al., 2012). Since *Neotoma* derive most of their water from their diet, this results in higher enamel $\delta^{18}\text{O}$ values. Jeffrey et al. (2015) showed a correlation between the $\delta^{18}\text{O}$ of rodent teeth and local environment, particularly in regions with high aridity, which could provide a complimentary dataset to $\delta^{13}\text{C}$ when reconstructing paleoenvironments that have experienced transitions to warmer, drier conditions.

Overall, isotope signals from small mammal teeth likely reflect both individual diets and surrounding environments (Figure 2) and have the potential to be sensitive indicators of local paleoclimate.

METHODS

STUDY SYSTEMS

We analyzed *Neotoma* sp. tooth fossils from two deposits which were excavated from Samwell Cave in northern California (Figure 1). Previous work done in the lab indicates these fossils are likely from *N. fuscipes* (Blois et al, unpublished data). Samwell Cave is located on the lower McCloud River of Shasta Lake and has a rich accumulation of small mammalian fossils from the late Pleistocene and Holocene (Blois et al., 2010; Feranec et al., 2010). The Samwell Cave Popcorn Dome (SCPD) deposit was excavated in 2007 and consists of 14 different levels of varying thicknesses (ranging from ~4cm to 10cm thickness; Blois et al. 2010), and documents an overall decline in the evenness and richness of small-mammal communities during the late Quaternary (Blois et al., 2010). The SCCUT (Samwell Cave Clara, Uma, and Tony) deposit was excavated in 2008 after observing promising fossil material on the surface. Over 3,000 bone and tooth samples were collected across ten 10cm thick stratigraphic levels within this deposit, with nearly 20 identified species (Blois et al, unpublished).

CHRONOLOGY OF CAVE DEPOSITS

This is the first time that samples from SCCUT have been described and analyzed, so we collected new radiocarbon dates (^{14}C) to investigate the timing of deposition. A total of 23 miscellaneous mammalian bones across all 10 levels, or deposition depth, of the SCCUT deposit were sent to the Keck-Carbon Cycle AMS facility at UC Irvine for radiocarbon analysis (Supplemental Table 1). The radiocarbon dates indicated substantial time averaging (see *Results*), with a break between Level 1 and all other levels of the deposit. Thus, we divided the deposit into two phases, and used OxCal (v4.4.4; Bronk Ramsey, 2001) to construct a chronology. We estimated the 95% confidence intervals of the older and younger boundaries of each phase using the OxCal Boundary() function, nesting the radiocarbon dates from individual specimens as a Phase() within the boundaries. Individual specimen ages were calibrated to IntCal20 (Reimer et al., 2020) using the R_Data() function. We then used the median boundary ages as our estimate of the older and younger ages of each phase (Supplemental Figure 1, Supplemental Table 2).

SCPD radiocarbon dates were initially analyzed by Blois et al (2010) and a chronology was inferred using the IntCal04 calibration curve (Reimer et al., 2004). We

created a new chronology for the SCPD deposit so that both deposits use the same calibration curve (Reimer et al., 2020). Since the SCPD deposits appear less mixed / bioturbated than the SCCUT deposit, and the dates are largely in stratigraphic order, we use the Bchron package (Haslett & Parnell, 2008) to calibrate our ^{14}C ages and develop an age-depth model (using the bchronology() function) for the SCPD deposit. We then used this chronology to infer the midpoint ages and uncertainty of all levels of the SCPD deposit (Figure 3, Supplemental Table 3).

STABLE ISOTOPE ANALYSIS

We analyzed the carbon and oxygen isotope composition from the tooth enamel of 66 *Neotoma* specimens (Supplemental Table 4): 38 specimens from SCCUT [26 RM1s, plus 12 additional pilot data specimens from other elements (8 Lm2 and 4 Rm2)] and 28 RM1 specimens from SCPD. For the primary SCPD dataset, we sampled the same element (RM1 – right upper 1st molars) so as not to inadvertently sample the same individual multiple times; SCCUT analyses and results include the pilot specimens but given taphonomic processes within cave deposits it is unlikely we are sampling the same individual multiple times (Behrensmeier et al., 2000) Since this study focuses on one species, we do not expect substantial variation in nitrogen values and therefore focus only on carbon and oxygen isotope composition as proxies for paleovegetation, paleodiet, and paleoenvironment.

The carbonate component of *Neotoma* tooth enamel was analyzed because enamel has been shown to preserve original isotopic composition in fossil specimens better than that of bone or dentin due to the chemical properties which make this material less susceptible to diagenetic alteration (Koch et al., 1997). Since this methodology is destructive, all fossil teeth used in this study were photographed and casts of each tooth were created for possible use in future morphometric studies. Working under a microscope, the enamel surface was removed from each tooth using a handheld Dremel drill with a 0.1 mm bit. Powdered enamel was collected on weigh paper and then transferred to 1.7 mL micro-centrifuge tubes. Extra precaution was taken during the drilling process to ensure that the powder being drilled off was pure enamel and not the dentin layer beneath. Dentin is more susceptible to alteration in fossil specimens and therefore could potentially alter our isotopic values if the powder we analyzed included a substantial portion of dentin, compared to enamel. There are distinct visual and physical differences between these two materials, with enamel being hard and more transparent than dentin, and so we are confident that any amount of dentin that might have been included is insignificant.

Enamel powder then underwent chemical pretreatment as detailed in (Koch et al., 1997). Each sample was treated with 1mL overnight of sodium hypochlorite (3% NaOCl) to remove organics. Samples were then centrifuged and rinsed with deionized water 5 times before adding 1mL of acetic acid (0.5M CH_3COOH) to remove any secondary carbonates. Samples were then rinsed 5 times with deionized water and dried overnight at 40°C. Enamel samples were analyzed via digestion with 110% phosphoric acid using a GasBench II coupled with a Delta V+ Plus Continuous Flow Isotope Ratio Mass Spectrometer (CF-IRMS) housed in the Stable Isotope Ecosystem Laboratory (SIELO) at UC Merced. Carbon and oxygen isotope compositions were corrected for instrument drift, mass linearity, and standardized to the international VPDB using the NBS 18 (n=10), USGS 44 (n=10), and an internal Carrara marble (n=10) reference

material. Analytical reproducibility for all reference materials was $\pm 0.1\%$. We also analyzed 7 aliquots of NIST 120C, a phosphorite with bulk chemistry similar to tooth enamel, as an internal check. Average isotope compositions for NIST 120C were $-6.6 \pm 0.2\%$ for $\delta^{13}\text{C}$, and $28.2 \pm 0.2\%$ for $\delta^{18}\text{O}$. All uncertainties are expressed as ± 1 standard deviation.

We then adjusted isotope values for trophic fractionation, accounting for the isotopic differentiation at each step of the food chain. The fractionation factor associated with these analyses depends on the preferential uptake of a lighter versus heavier isotope during biochemical reactions of nutrient assimilation, which will ultimately determine how enriched or depleted a pool is with one isotope relative to the other (i.e., ^{13}C vs ^{12}C). We calculated the $\delta^{13}\text{C}$ values of the animals diet using an enamel-diet enrichment factor (ϵ) of 11.5% (Passey et al., 2005) and corrected for changes to the $\delta^{13}\text{C}$ of the atmosphere (Suess effect) by subtracting 1.5% to estimate $\delta^{13}\text{C}_{\text{diet}}$. The $\delta^{18}\text{O}$ data was also standardized relative to the Pee Dee Belemnite standard (VPDB) but were converted to Standard Mean Ocean Water (SMOW) to allow for comparison with water isotope data and other proxies using the equation $\delta^{18}\text{O}_{\text{SMOW}} = 1.03 * \delta^{18}\text{O}_{\text{PDB}} + 30.91$ (Coplen et al., 1983). Isotopic analysis is reported in delta notation (δ) and expressed in parts-per-mil ($\%$), based on the equation $d = [(R_{\text{sample}}/R_{\text{standard}}) - 1] * 1000$, where R represents the molar ratio of the heavy over lighter stable isotopes of the sample being analyzed and the corresponding standard. For carbon the ratio is $^{13}\text{C}/^{12}\text{C}$ and the oxygen ratio is $^{18}\text{O}/^{16}\text{O}$.

STATISTICAL ANALYSIS: VARIATION IN SCPD STABLE ISOTOPE VALUES THROUGH TIME

Because the SCCUT deposit was temporally mixed (see *Results*), we focused on SCPD for statistical analyses of change-through-time. Given that our sample size per level varied and some deposit levels had no raw isotope values, we used two models that capture different assumptions about how isotope values changed through time. Model 1 is a linear regression model with the stable isotope composition as the dependent variable and age as the independent variable. This model is useful for examining the overall trend in isotope values. Model 2 is a piecewise linear interpolation model, where linear interpolation was performed between mean isotope values for each deposit level through time (Table 1). This model is most closely aligned with the raw data from each analyzed level, though it also infers mean isotope values for two unsampled levels (Level e2 and e6b) and may over-interpret temporal variability in isotope values given the small sample size per level. For the purposes of interpreting major trends in carbon and oxygen values through time at Samwell Cave, we rely primarily on Model 1.

STATISTICAL ANALYSIS: CORRESPONDENCE BETWEEN SCPD AND OTHER PROXIES

We compared SCPD $\delta^{18}\text{O}$ values from both the regression model ($\delta^{18}\text{O}_{\text{SCPD-R}}$) and the interpolation model ($\delta^{18}\text{O}_{\text{SCPD-I}}$) with global and regional climate data. The global climate proxy dataset consists of $\delta^{18}\text{O}$ values from the NGRIP ice core ($\delta^{18}\text{O}_{\text{NGRIP}}$; North Greenland Ice Core Project members, 2004). Regional data were drawn from two speleothem records recovered from caves in California: Moaning Cavern and Lake Shasta Cavern ($\delta^{18}\text{O}_{\text{MS}}$, $\delta^{18}\text{O}_{\text{LSC}}$, see Figure 1) (Oster et al., 2009, 2020). For all proxy records, we determined the age range of each SCPD level by calculating the age \pm standard deviation from the inferred age model (Supplemental Table 3), matched all the original proxy data within the age range for each level, and then calculated the mean

proxy value for that time bin. We then performed Pearson's correlation tests to determine correspondence between SCPD $\delta^{18}\text{O}$ values (inferred from both Model 1 and Model 2), and the $\delta^{18}\text{O}$ proxy data.

We used the same method to compare $\delta^{13}\text{C}$ values from our regression model and interpolation model carbon ($\delta^{13}\text{C}_{\text{SCPD-R}}$, $\delta^{13}\text{C}_{\text{SCPD-I}}$) to regional and global proxy records. For global trends in carbon, we relied on atmospheric CO_2 concentrations (ppm) extracted from the Byrd ice core in Antarctic (Pedro et al., 2012). For a more direct comparison of trends in carbon isotope changes from the same genus during the same time period, we compared SCPD $\delta^{13}\text{C}$ values from *Neotoma* analyzed by Tomé et al. (2021), though these $\delta^{13}\text{C}$ values were taken from tooth collagen. We corrected all values from Tomé et al (2021) for collagen-diet fractionation (Koch et al., 1997; Lee-Thorp et al., 1989). We then calculated Pearson's correlation coefficient to determine correspondence between SCPD $\delta^{13}\text{C}$ values from both Model 1 and Model 2, and the two carbon proxy data sets.

Overall, six correlation tests were run using our two SCPD $\delta^{18}\text{O}$ models against NGRIP ($\delta^{18}\text{O}_{\text{NGRIP}}$) data and speleothem data from two cave sites in northern California (Moaning Cavern, $\delta^{18}\text{O}_{\text{MC}}$; Lake Shasta Cavern, $\delta^{18}\text{O}_{\text{LSC}}$). An additional four correlation tests were conducted using the two SCPD $\delta^{13}\text{C}$ models against atmospheric CO_2 values and *Neotoma* $\delta^{13}\text{C}$ isotope values from Tomé et al. (2021) ($\delta^{13}\text{C}_{\text{Tomé}}$) (Table 2). All analyses were done with R (R: A language and environment for statistical computing, 2020; Version 1.3.1093).

RESULTS

RADIOCARBON DATES & CHRONOLOGY

SCPD

The SCPD deposit has a relatively linear relationship between deposit depth and age except for one sample (Figure 3). The new age model predicts ages for each level that differ somewhat from the original age model (Blois et al., 2010; Supplemental Table 3). However, our new model provides a better estimate of error and relies on a more recent calibration curve, so we used this new age model for all deposit depth ages.

SCCUT

Only 9 out of the 23 SCCUT samples produced enough collagen to be viable for ^{14}C analysis (Supplemental Table 1). The low collagen yield speaks to the lack of preservation at this deposit, likely due to its more exposed location at the mouth of the cave. There is strong time-averaging across deposit levels (Supplemental Figure 1), so we were unable to develop a high-resolution chronology for this dataset. However, there appear to be two separate time periods within the deposit (i.e., there is a gap in radiocarbon dates between Level 1 and the other levels), and we used this separation to group radiocarbon dates into two time-bins: Level 1 and all other levels. The boundary ages for SCCUT inferred from OxCal for these two groups indicate a (mostly) late Pleistocene depositional phase extending from 25,480 cal BP to 9057 cal BP, and a

Holocene phase extending from 9057 cal BP to the present (Supplemental Table 2). Given the time averaged nature of SCCUT, we focus on the SCPD data for the remainder of the manuscript, examining SCCUT data for consistency with patterns seen in SCPD.

VARIATION IN STABLE ISOTOPES VALUES THROUGH TIME

SCPD

The SCPD $\delta^{13}\text{C}_{\text{diet}}$ values range from -18.2‰ to -29.1‰ (Figure 4, Table 1, Supplemental Table 4). All the isotope values fall squarely within the established range for C_3 plants. There is not a statistically significant relationship between $\delta^{13}\text{C}_{\text{diet}}$ and age (Model 1: $F_{(1,26)}=1.391$, Adj. $R^2 = 0.014$, $p=0.249$). Before accounting for the enamel-diet fractionation, raw $\delta^{13}\text{C}_{\text{enamel}}$ values range from -16.4‰ to -5.4‰.

The SCPD $\delta^{18}\text{O}_{\text{SMOW}}$ values range from 21.8‰ to 28.1‰ with a trend showing lower values in older time periods and higher values in more recent time periods (Figure 4). There is a significantly positive relationship between $\delta^{18}\text{O}_{\text{enamel}}$ and age based on linear regression (Model 1: $F_{(1,26)}=6.056$, Adj. $R^2 = 0.158$, $p=0.021$).

SCCUT

The $\delta^{13}\text{C}_{\text{diet}}$ values have an overall range from -29.4‰ to -17.0‰. The mean value of the Late Pleistocene group is -22.6‰ and the mean value from the Holocene group is -27.3‰ (Supplemental Figure 2); the difference between time periods is statistically significant ($t=-7.54$, $df = 15.23$, $p < 0.001$). As seen in SCPD, the values all fall within the established range of C_3 plants which gives further confidence to the assumption that *Neotoma* were living and feeding in a predominantly C_3 environment over the last 22 kya. The $\delta^{18}\text{O}_{\text{enamel}}$ values range from 23.3‰ to 31.8‰, with a mean value of 26.6‰ for the Late Pleistocene group and 27.9‰ for Holocene. These data show the same pattern of moving towards higher values (warmer temperatures) during the Holocene; there is a 1.3‰ difference between the lower mean Pleistocene values and the higher Holocene values, though this was not statistically significant ($t = 1.62$, $df = 9.39$, $p = 0.1393$). Additionally, carbon and oxygen values from the same specimens within SCCUT were significantly correlated ($r=-0.5655$, $p = 0.0002$).

CORRESPONDENCE AMONG SCPD AND OTHER PALEOENVIRONMENTAL PROXIES

OXYGEN:

MODEL 1: LINEAR REGRESSION

The $\delta^{18}\text{O}_{\text{SCPD-R}}$ values inferred from Model 1 were significantly correlated with the global ($\delta^{18}\text{O}_{\text{NGRIP}}$) proxy data (Table 2, Figure 5). $\delta^{18}\text{O}_{\text{SCPD-R}}$ values showed a significant negative correlation with $\delta^{18}\text{O}_{\text{LSC}}$ values but no correlation with $\delta^{18}\text{O}_{\text{MC}}$ values (Table 2, Figure 5).

MODEL 2: LINEAR INTERPOLATION

The $\delta^{18}\text{O}_{\text{SCPD-I}}$ values inferred from the interpolation model did not show any significant relationships with the global or regional climate data (Table 2, Figure 5).

CARBON:

MODEL 1: LINEAR REGRESSION

The $\delta^{13}\text{C}_{\text{SCPD-R}}$ values inferred from linear regression model for carbon were significantly correlated with atmospheric CO_2 , and marginally not significantly correlated with the $\delta^{13}\text{C}_{\text{Tomé}}$ values (Table 2, Figure 5).

MODEL 2: LINEAR INTERPOLATION

The $\delta^{13}\text{C}_{\text{SCPD-I}}$ values inferred from the interpolation model did not show any significant relationships with atmospheric CO_2 or $\delta^{13}\text{C}_{\text{Tomé}}$ data (Table 2, Figure 5).

DISCUSSION

We sought to quantify changes in stable carbon ($\delta^{13}\text{C}$) and oxygen ($\delta^{18}\text{O}$) isotope compositions from *Neotoma* teeth as potential indicators of late Quaternary environmental conditions. We showed that both $\delta^{18}\text{O}_{\text{enamel}}$ and $\delta^{13}\text{C}_{\text{enamel}}$ exhibited change through time that corresponded with the global transition from glacial to an interglacial period. However, more local and temporally dynamic interpretation of paleoclimate was more difficult. Overall, more data per time period and/or individually dated specimens paired with isotopes, combined with more detailed knowledge of isotopic linkages along the atmosphere-plant-small mammal pathway would be needed to improve spatially and temporally local interpretations.

CHANGE IN CARBON ISOTOPE VALUES THROUGH TIME

There is overall very little change in carbon isotope composition through time, reflecting environmental stability and C_3 dominated ecosystem during the late Quaternary: both SCPD and SCCUT deposits exhibit a slight overall transition from higher $\delta^{13}\text{C}$ values in the late Pleistocene to lower $\delta^{13}\text{C}$ values into the Holocene, but this trend was not significant (Figure 4, Supplemental Figure 2). Previous research has suggested that within the C_3 range of values, higher values (-26 to -22‰) reflect a drier ecosystem with mean annual precipitation of less than 1000 mm/yr (Kohn, 2010). All of the SCPD $\delta^{13}\text{C}$ values prior to 13 kya fall within that range and all SCCUT $\delta^{13}\text{C}$ values grouped as Late Pleistocene are greater than -27‰, potentially reflecting a drier ecosystem. This interpretation agrees with regional speleothem data that shows drier conditions in northern California from 21–14 kya, and then wetter conditions from 11 – 8 kya (Oster et al., 2009, 2020) which is broadly reflected in the more negative SCPD and SCCUT $\delta^{13}\text{C}$ values observed in the Holocene.

The relative stability of carbon through time is puzzling, given the known substantial changes in regional plant communities (Whitlock & Bartlein, 1997; Mohr et al., 2000; Scott Anderson et al., 2008). Based on fossil pollen data from this region, over the last 20 kya there was a shift from subalpine parkland to pine and oak forests, and then a further shift to present-day conditions of Douglas-fir, ponderosa pine, and oak woodlands (Whitlock & Bartlein, 1997; Mohr et al., 2000). Plant community changes, however, were largely transitions from one C_3 dominated assemblage to a different C_3

plant dominated assemblage, so the major vegetation changes may not be reflected in carbon isotope values incorporated into *Neotoma* tooth enamel. But, even within a pure C₃ environment, changes in environmental conditions (i.e., atmospheric CO₂, water availability, light, temperature) can influence the carbon isotopic composition of plants and therefore the $\delta^{13}\text{C}_{\text{diet}}$ values from tooth enamel (Heaton, 1999; Kohn, 2010). Lower $\delta^{13}\text{C}$ values have been associated with shaded and humid environments, ranging as low as -32‰ (van der Merwe & Medina, 1991; Gehler et al., 2012) and higher values are linked to open, arid environments (Ehleringer & Cooper, 1988; Jeffrey et al., 2015). This aligns with regional climate proxies that show drier conditions during the Late Pleistocene and increased moisture into the Holocene, reflected in our dataset as slightly more negative $\delta^{13}\text{C}_{\text{diet}}$ values after 10 kya.

Indeed, despite the lack of significant change in carbon at SCPD through time, $\delta^{13}\text{C}_{\text{diet}}$ values were significantly correlated with trends in atmospheric CO₂ (Table 2), reflecting the overall transitions from glacial to interglacial cycles. The relationship between atmospheric CO₂ and $\delta^{13}\text{C}_{\text{diet}}$ values is especially complicated due to the multi-step fractionation between plant uptake and herbivore consumption, but previous research has shown an increase in atmospheric CO₂ concentration corresponds to a decrease in $\delta^{13}\text{C}_{\text{diet}}$ values (Podlesak et al., 2008; Clementz, 2012). Indeed, we also see an inverse and significant correlation between *Neotoma* $\delta^{13}\text{C}_{\text{SCPD-R}}$ values and atmospheric CO₂, indicating that *Neotoma* roughly track global atmospheric changes through their plant consumption. However, reconciling the potential roles of vegetation and climate on *Neotoma* isotope values is difficult without a more detailed record of shifts in isotopic composition of paleovegetation from the late Quaternary. Further, because we do not see a correlation between $\delta^{13}\text{C}_{\text{SCPD-I}}$ and atmospheric CO₂ values (Table 2), this may be a spurious result due to correlating two time series.

Previously published isotopic data on *Neotoma* from the same time period shows a similar story of isotopic stability with most $\delta^{13}\text{C}_{\text{diet}}$ values plotting within a C₃ environment, and a progression towards more positive values into the Holocene (Tomé et al., 2022). The range of $\delta^{13}\text{C}_{\text{diet}}$ values for *Neotoma* from Tomé et al. (2021) is slightly higher than our values from SCPD *Neotoma* (-26.42 to -13.26‰) which is not surprising since their study site is located in central Texas, a more arid environment with a much higher abundance of C₄ plants during the late Pleistocene, but the overlap of ranges is consistent with what we would expect. Tomé et al (2021) also used change in *Neotoma* body mass as a proxy for climate variation and found that a decrease in body size during the early Holocene correlated with an increase in temperature and precipitation. This paleoclimatic shift towards a warmer and wetter environment is also shown in our data as well as other proxy data from Northern California.

CHANGE IN OXYGEN ISOTOPE VALUES THROUGH TIME

In general, lower $\delta^{18}\text{O}$ values are associated with cooler temperatures, whereas warmer temperatures result in preferential evaporation of the lighter ¹⁶O isotope which produces higher $\delta^{18}\text{O}$ values (Sponheimer & Lee-Thorp, 1999; Delagye, 2009). At SCPD, oxygen isotope values from *Neotoma* teeth changed significantly through time, reflecting a warmer climate as the Earth system transitioned into the Holocene; which was observed in both the SCPD and SCCUT records (Figure 4, Supplemental Figure 2). The overall trend is consistent with the inferred North Greenland Ice Core (NGRIP)

temperatures (Figure 5, Table 2). Previous research has suggested that a 1‰ difference in $\delta^{18}\text{O}$ isotopes reflects a 4°C change in temperature (Delaygue, 2009) which suggests from 5.4 – 10.36°C change at Samwell Cave: e.g., SCCUT saw a 1.35‰ difference between the time-averaged Late Pleistocene and Holocene $\delta^{18}\text{O}$ values, and there was a roughly 2.5‰ difference in $\delta^{18}\text{O}$ isotope values between the two oldest LGM samples and the two youngest late Holocene samples at SCPD. Further, the lowest SCPD $\delta^{18}\text{O}$ values all occur prior to 15 kya when the Bølling-Allerød warming event began, consistent with expectations based on known paleoclimate trends. However, the lack of relationship between the *Neotoma* $\delta^{18}\text{O}_{\text{SCPD-I}}$ values from the interpolation model and the NGRIP record indicates that *Neotoma* isotope values are not tracking closely the dynamic climate changes that we know occurred throughout the late Quaternary, such as the rapid increase in temperature during the Bølling-Allerød followed by the rapid drop in temperature during the Younger Dryas. Overall, SCPD $\delta^{18}\text{O}_{\text{SCPD-R}}$ reflects the broad-scale warming trends from a glacial to interglacial transitions.

Paleotemperature can be challenging to decipher from mammal proxy records, due to their endothermic nature (i.e., constant body temperature) without additional proxies (Eberle et al., 2010; Grimes et al., 2004). Therefore, trends in $\delta^{18}\text{O}$ may better reflect changes in regional aridity / precipitation sourcing rather than global temperature. Changes in $\delta^{18}\text{O}$ values due to increased aridity occur through enrichment of ^{18}O in leaf matter, which could subsequently have been recorded in *Neotoma* enamel (McLean & Emslie, 2012; Jeffrey et al., 2015). Based on the regional climate data from fossil pollen and speleothems, environmental conditions were drier prior to 15 kya (Oster et al., 2020) but believed to be cooler during that same time frame (Daniels et al., 2005).

Since speleothems are often reflective of hydroclimate (Tooth & Fairchild, 2003; Tremaine & Froelich, 2013), we compared $\delta^{18}\text{O}$ at SCPD with two local/regional speleothem records (Figure 1). However, correlations between SCPD $\delta^{18}\text{O}$ and the speleothem records were inconsistent. We found a significant relationship between $\delta^{18}\text{O}_{\text{SCPD-R}}$ values and $\delta^{18}\text{O}$ values from Lake Shasta Caverns, but not between $\delta^{18}\text{O}_{\text{SCPD-R}}$ and Moaning Caverns $\delta^{18}\text{O}$ values. However, the significant relationship at Lake Shasta Caverns was negative, indicating an anti-correlation between the two records. The Lake Shasta Caverns record does not encompass the Holocene interglacial, so it truncates the amount of climate change seen. Further, the precipitation patterns seen at Lake Shasta Caverns are complex, reflecting changes in temperature, regional water origin, and water transport (Oster et al., 2020), so interpretation of what this means for *Neotoma* isotope values at SCPD is not straightforward. The isotopic patterns at Moaning Caverns, which encompasses the latest Pleistocene and early Holocene, are broadly consistent with trends in $\delta^{18}\text{O}$ at SCPD but not significant, likely due to the low sample size caused by the shortness of the Moaning Caverns record (Figure 5).

Overall, using speleothems to help interpret *Neotoma* oxygen isotope composition is potentially useful because the two proxies broadly reflect the same spatial scales. However, differences in the interpretation of the speleothems (e.g., Oster et al 2020) and temporal features of the records (i.e., the speleothem records are high-resolution but short whereas the *Neotoma* SCPD record is time-averaged by longer) makes comparison difficult in this case.

SCCUT

The SCCUT deposit is highly time-averaged (Supplemental Figure 1) and so the stable isotope data from SCCUT lacks the temporal controls of the SCPD dataset. However, changes in isotopes between Late Pleistocene and Holocene groups at SCCUT are consistent with SCPD isotope trends, supporting the overall patterns we've shown here. The $\delta^{13}\text{C}_{\text{enamel}}$ values from SCCUT are consistent with a C_3 environment but show a strong separation between the Pleistocene and Holocene, with higher values observed during the Late Pleistocene and a transition to lower values during the Holocene. This corresponds with SCPD $\delta^{13}\text{C}_{\text{enamel}}$ values and the environmental conditions described by regional climate proxies (Daniels et al., 2005; Oster et al., 2009, 2020). The SCCUT $\delta^{18}\text{O}$ values also broadly mirror the trend seen in the SCPD deposit, with a shift to higher values throughout the late Quaternary indicating a warming environment. Carbon and oxygen values from the same SCCUT specimens also show a strong correlation to each other ($r = -0.5655$, $p = 0.0002$), suggesting these two datasets have a statistically significant relationship to each other. Previous research has suggested this could indicate seasonality or climate-based interactions (Kohn & McKay, 2012) but without a strong age model it is challenging to test the significance of this correlation because we cannot compare SCCUT data to other environmental proxies.

CONCLUSIONS

Small mammals are known for being valuable recorders of conditions in localized regions (e.g., Porder et al., 2003), and track changes that are more spatially sensitive when compared to global scale proxies such as ice cores. Overall, our data show that the tooth enamel isotopes from *Neotoma* track global changes in carbon and oxygen associated with the transition from glacial to interglacial cycles but interpreting our data relative to local scale and temporally dynamic environmental changes is more challenging. This is largely due to the limitations of the Samwell Cave *Neotoma* isotope datasets, as well as discrepancies between the relative strengths and weaknesses of different proxies: the *Neotoma* sample size per time bin were relatively small, and the extent of time averaging in the SCPD deposit relatively large, especially compared to ice core and speleothem data. The Moaning Cave and Lake Shasta Caverns speleothem records only overlap a small portion of the SCPD time period, limiting sample sizes even further for comparisons between SCPD and speleothems. Ultimately, our study system shows promise in small mammal isotopes as a paleoenvironmental record, but further research to bolster sample sizes and improve temporal resolution of the Samwell Cave deposits is needed.

TABLES AND FIGURES

Table 1. Isotope values from the SCPD deposit by level. Shown are the number (*n*) of samples per level, with the minimum (min), maximum (max), and mean isotope value per level calculated for both carbon ($\delta^{13}\text{C}$) and oxygen ($\delta^{18}\text{O}$) isotopes.

| Level | <i>n</i> of samples | $\delta^{13}\text{C}_{\text{PDB}}$ (‰) | | | $\delta^{18}\text{O}_{\text{SMOW}}$ (‰) | | |
|-------|---------------------|--|-------|-------|---|------|------|
| | | min | mean | max | min | mean | max |
| 1 | 1 | -16.4 | -16.4 | -16.4 | 26.7 | 26.7 | 26.7 |
| 3a | 3 | -10.5 | -11.8 | -13.4 | 26.1 | 26.1 | 27.1 |
| 3b | 1 | -7.3 | -7.3 | -7.3 | 25.1 | 25.1 | 25.1 |
| 4a | 3 | -5.7 | -11.1 | -13.9 | 23.9 | 25.4 | 28.2 |
| 4b | 3 | -10.1 | -12.0 | -14.3 | 25.8 | 26.6 | 27.1 |
| 5a | 2 | -7.7 | -9.5 | -11.2 | 23.7 | 24.1 | 24.6 |
| 5b | 2 | -12.2 | -13.6 | -14.9 | 24.9 | 25.2 | 25.5 |
| 6a | 1 | -9.6 | -9.6 | -9.6 | 26.8 | 26.8 | 26.8 |
| 7a | 1 | -5.4 | -5.4 | -5.4 | 26.8 | 26.8 | 26.8 |
| 7b | 5 | -8.9 | -10.7 | -13.4 | 21.8 | 24.9 | 27.3 |
| 8a | 2 | -10.5 | -11.0 | -11.5 | 23.1 | 24.1 | 25.1 |
| 8b | 3 | -10.4 | -10.6 | -10.9 | 22.2 | 23.6 | 24.8 |

Table 2. The relationship between carbon and oxygen isotope values at SCPD and other proxies. Two models for the SCPD isotope values (Model 1: linear regression; Model 2: linear interpolation) were used to make the comparisons. Shown are the Pearson's correlation coefficient (r), the number (n) of samples for each comparison, and the p -value. Asterisk (*) on p -values and bolded model indicates a statistically significant model.

| Model | Correlation coefficient | n of samples | p-value |
|---|-------------------------|--------------|----------------|
| $\delta^{18}\text{O}_{\text{SCPD-R}} \sim \delta^{18}\text{O}_{\text{NGRIP}}$ | 0.9131 | 14 | 0.0000* |
| $\delta^{18}\text{O}_{\text{SCPD-I}} \sim \delta^{18}\text{O}_{\text{NGRIP}}$ | 0.2953 | 14 | 0.3053 |
| $\delta^{18}\text{O}_{\text{SCPD-R}} \sim \delta^{18}\text{O}_{\text{MC}}$ | 0.6251 | 7 | 0.1333 |
| $\delta^{18}\text{O}_{\text{SCPD-I}} \sim \delta^{18}\text{O}_{\text{MC}}$ | -0.1182 | 7 | 0.8006 |
| $\delta^{18}\text{O}_{\text{SCPD-R}} \sim \delta^{18}\text{O}_{\text{LSC}}$ | -0.9112 | 5 | 0.0313* |
| $\delta^{18}\text{O}_{\text{SCPD-I}} \sim \delta^{18}\text{O}_{\text{LSC}}$ | -0.8053 | 5 | 0.1000 |
| $\delta^{13}\text{C}_{\text{SCPD-R}} \sim \text{CO}_2$ (ppm) | -0.9497 | 10 | 0.0000* |
| $\delta^{13}\text{C}_{\text{SCPD-I}} \sim \text{CO}_2$ (ppm) | -0.2600 | 10 | 0.4680 |
| $\delta^{13}\text{C}_{\text{SCPD-R}} \sim \delta^{13}\text{C}_{\text{Tomé}}$ | -0.5518 | 11 | 0.0784 |
| $\delta^{13}\text{C}_{\text{SCPD-I}} \sim \delta^{13}\text{C}_{\text{Tomé}}$ | -0.1895 | 11 | 0.5767 |



Figure 1. Location of Samwell Cave in northern California (red star). Also shown are the locations of two speleothem datasets (yellow circles), Moaning Caverns (Oster et al. 2009) and Lake Shasta Caverns (Oster et al. 2020). Map colors represent mammal species richness, dark green is highest richness and light brown is lowest richness (California Department of Fish & Game, 2003)

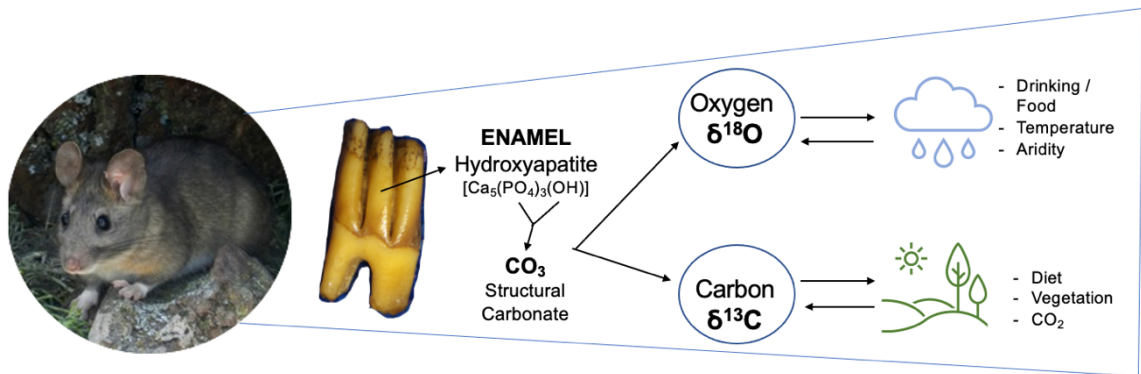


Figure 2. Conceptual systems diagram showing an overview of the study system; *Neotoma* tooth enamel to oxygen and carbon isotopes recorded through interactions with surrounding environments. The image of *Neotoma* is ©Soheil Zendeh (sohzenh, CC BY-NC-SA 4.0, retrieved from www.inaturalist.org).

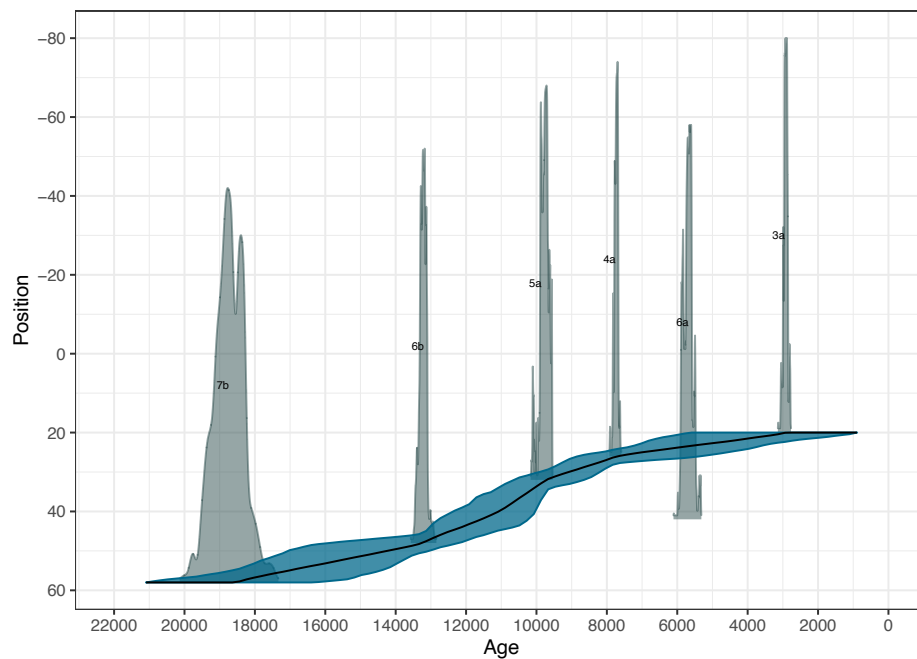


Figure 3. The updated SCPD age model, created using the Bchron package (Haslett & Parnell, 2008) in R (*R: A Language and Environment for Statistical Computing*, 2020). The x-axis (Age) is calibrated years before present and the y-axis (Position) indicates depth of each radiocarbon date in centimeters (corresponding to the base of the calibrated radiocarbon date distribution). Gray shading indicates the calibrated radiocarbon age distribution, the black line is the inferred mean age across depth, and blue shading indicates error of the inferred age at each depth.

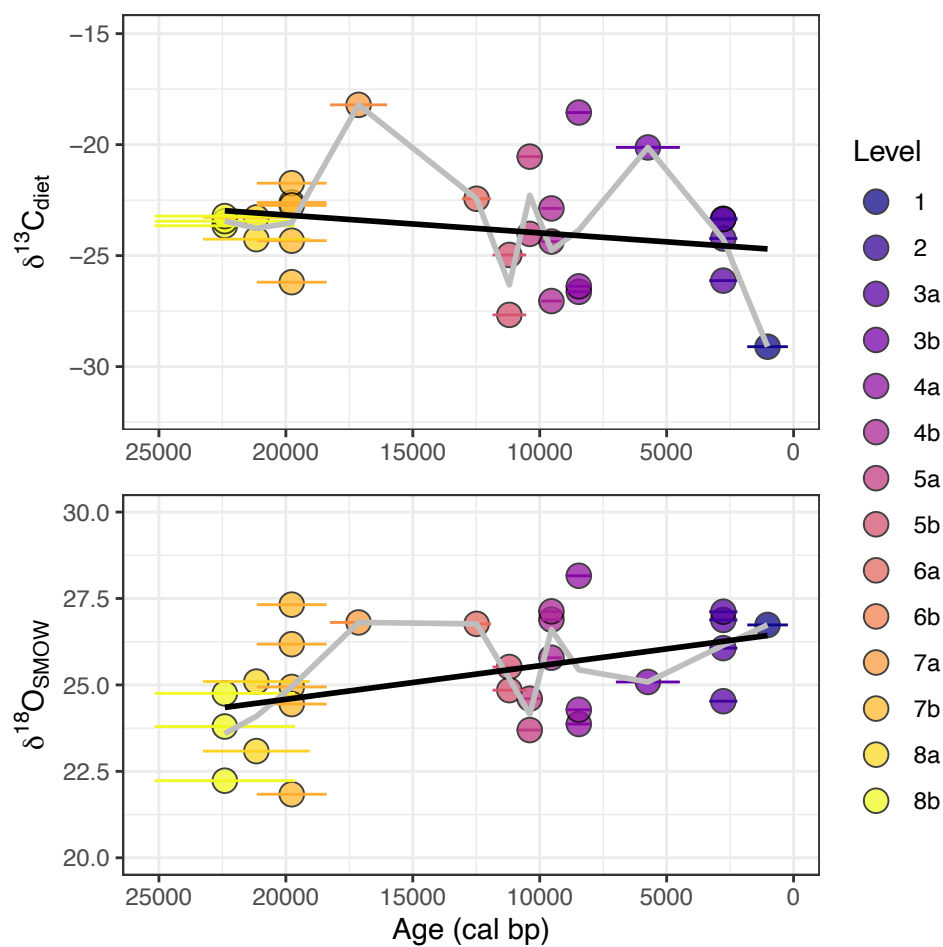


Figure 4. SCPD isotope values by level (colors) and age (x-axis). Error bars represent standard deviation from the age model and the lines represent the two linear models that were created; the black line is Model 1 linear regression, and the grey line is Model 2 linear interpolation. For Carbon, there is not a statistically significant relationship between $\delta^{13}\text{C}_{\text{diet}}$ and age (Model 1: $F_{(1,26)}=1.391$, Adj. $R^2 = 0.014$, $p=0.249$). For Oxygen, there is a significantly positive relationship between $\delta^{18}\text{O}_{\text{SMOW}}$ and age (Model 1: $F_{(1,26)}=6.056$, Adj. $R^2 = 0.158$, $p=0.021$).

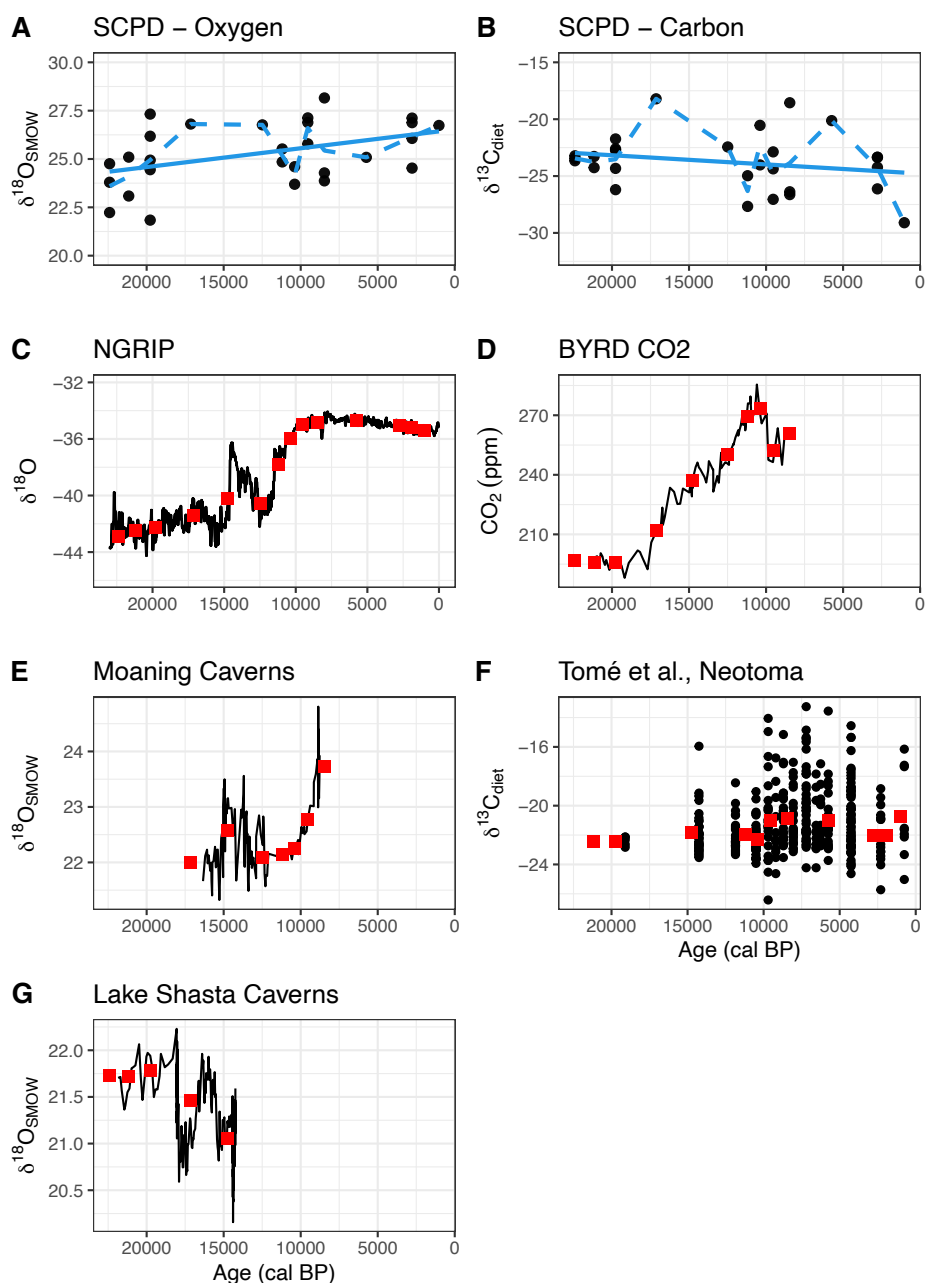


Figure 5. SCPD isotope data compared with climate proxies; red squares are the data points that were used in correlation analyses (red points are binned averages), black dots/lines are raw data. A) SCPD $\delta^{18}\text{O}_{\text{SMOW}}$ values with linear regression model 1 (solid blue line) and linear interpolation model 2 (dashed blue line), B) SCPD $\delta^{13}\text{C}_{\text{diet}}$ values with linear regression model 1 (dashed blue line) and linear interpolation model 2 (solid blue line), C) $\delta^{18}\text{O}$ temperature data from North Greenland Ice Core (North Greenland Ice Core Project members, 2004), D) atmospheric CO₂ data (ppm) from Byrd ice core in Antarctica (Pedro et al., 2012), E) speleothem $\delta^{18}\text{O}$ data from Moaning Cavern (Oster et al., 2009) F) published $\delta^{13}\text{C}_{\text{diet}}$ data from *Neotoma* in Texas (Tomé et al., 2021) and G) speleothem $\delta^{18}\text{O}$ data from Lake Shasta Cavern (Oster et al., 2020).

SUPPLEMENTAL TABLES AND FIGURES

Supplemental Table 1 Radiocarbon dates from SCCUT bone samples, analyzed at the UC Irvine Keck AMS lab (UCIAMS).

| Specimen ID | UCIAMS | Element | Measured ^{14}C age (BP) | Excavation Level | Collagen Yield (%) | C:N (atomic) |
|-------------|--------|---------|-----------------------------------|------------------|--------------------|--------------|
| DAF 711 | 253887 | Tibia | 215 \pm 15 | 1 | 5.6 | 3.4 |
| DAF 710 | 254890 | Humerus | 4,135 \pm 15 | 1 | 3.6 | 3.6 |
| DAF 600 | 254891 | Humerus | 9,935 \pm 25 | 2 | 0.8 | 3.5 |
| DAF 659 | 253888 | Radius | 12,130 \pm 30 | 2 | 3.5 | 3.5 |
| DAF 663 | 253889 | Tibia | 19,770 \pm 70 | 4 | 2 | 3.5 |
| DAF 706 | 253890 | Radius | 20,420 \pm 80 | 6 | 2.9 | 3.5 |
| DAF 709 | 254892 | Radius | 13,505 \pm 50 | 6 | 3.4 | 3.4 |
| DAF 666 | 253891 | Tibia | 12,250 \pm 40 | 8 | 0.7 | 3.4 |
| DAF 722 | 253892 | Humerus | 10,620 \pm 30 | 9 | 0.9 | 3.4 |

Supplemental Table 2. Updated age model for each level of the SCCUT deposit. Indicated are the modelled ages for each boundary and/or individual date in calibrated years BP. The mean, standard deviation (SD), and median age of each estimate is also shown. Relevant ages of the boundaries between the two temporal phases are bolded.

| | From | To | Mean | SD | Median |
|------------------------|-------------|-----------|-------------|-----------|---------------|
| Top Boundary | 298 | -8199 | -2160 | 2589 | -1184 |
| Holocene Phase | | | | | |
| R_Date DAF 710 | 302 | 3 | 208 | 74 | 176 |
| R_Date DAF 711 | 4816 | 4575 | 4687 | 74 | 4680 |
| Break Boundary | 11352 | 4838 | 8695 | 1914 | 9057 |
| Late Pleistocene Phase | | | | | |
| R_Date DAF 659 | 14100 | 13862 | 14013 | 68 | 14041 |
| R_Date DAF 600 | 11598 | 11246 | 11335 | 64 | 11322 |
| R_Date DAF 663 | 23943 | 23424 | 23788 | 109 | 23807 |
| R_Date DAF 706 | 24832 | 24220 | 24509 | 159 | 24506 |
| R_Date DAF 709 | 16481 | 16097 | 16284 | 90 | 16283 |
| R_Date DAF 666 | 14765 | 14057 | 14190 | 131 | 14158 |
| R_Date DAF 722 | 12718 | 12506 | 12652 | 48 | 12662 |
| Bottom Boundary | 30498 | 24218 | 26219 | 2255 | 25480 |

Supplemental Table 3. Updated age model for each level created from the SCPD deposit radiocarbon dates. The depth is the midpoint depth from each level, in centimeters, and the ages of each level are in calibrated years before present (cal BP). Also shown is the estimated midpoint age from the age model in Blois et al. 2010.

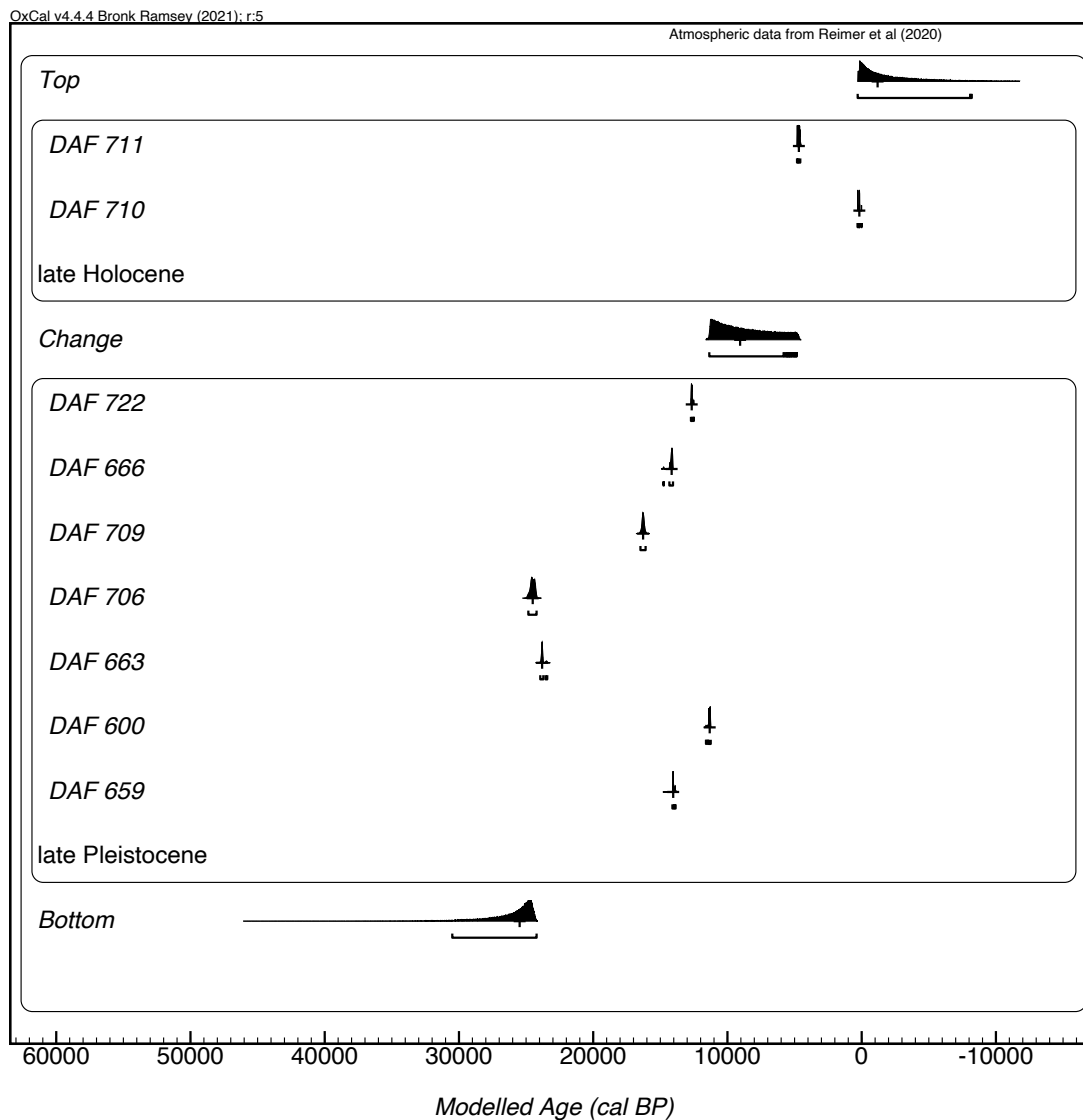
| Mid-Depth | Level | Age (cal BP) | ± SD | Blois et al. 2010 age |
|------------------|--------------|-------------------------|-------------|----------------------------------|
| 1 | e1 | 1,025 | 800 | 752 |
| 11 | e2 | 1,898 | 695 | 2,758 |
| 18.5 | e3a | 2,770 | 554 | 4,639 |
| 23.5 | e3b | 5,740 | 1,259 | 5,893 |
| 28 | e4a | 8,461 | 469 | 7,021 |
| 31.5 | e4b | 9,538 | 402 | 7,899 |
| 35.5 | e5a | 10,393 | 454 | 8,902 |
| 40.5 | e5b | 11,197 | 663 | 10,156 |
| 45.5 | e6a | 12,487 | 576 | 11,410 |
| 50.5 | e6b | 14,745 | 1,102 | 12,664 |
| 55.5 | e7a | 17,137 | 1,123 | 13,918 |
| 60.5 | e7b | 19,769 | 1,377 | 15,172 |
| 65.5 | e8a | 21,162 | 2,104 | 16,425 |
| 70.5 | e8b | 22,405 | 2,765 | 17,679 |

Supplemental Table 4. All *Neotoma* fossil specimens included in the study, collected from two sites within Samwell Cave in Shasta County, CA. Shown are the original specimen ID, the deposit and level within the deposit, the element from which tooth enamel was sampled, and the measured stable carbon ($\delta^{13}\text{C}$) and oxygen ($\delta^{18}\text{O}$) isotope values.

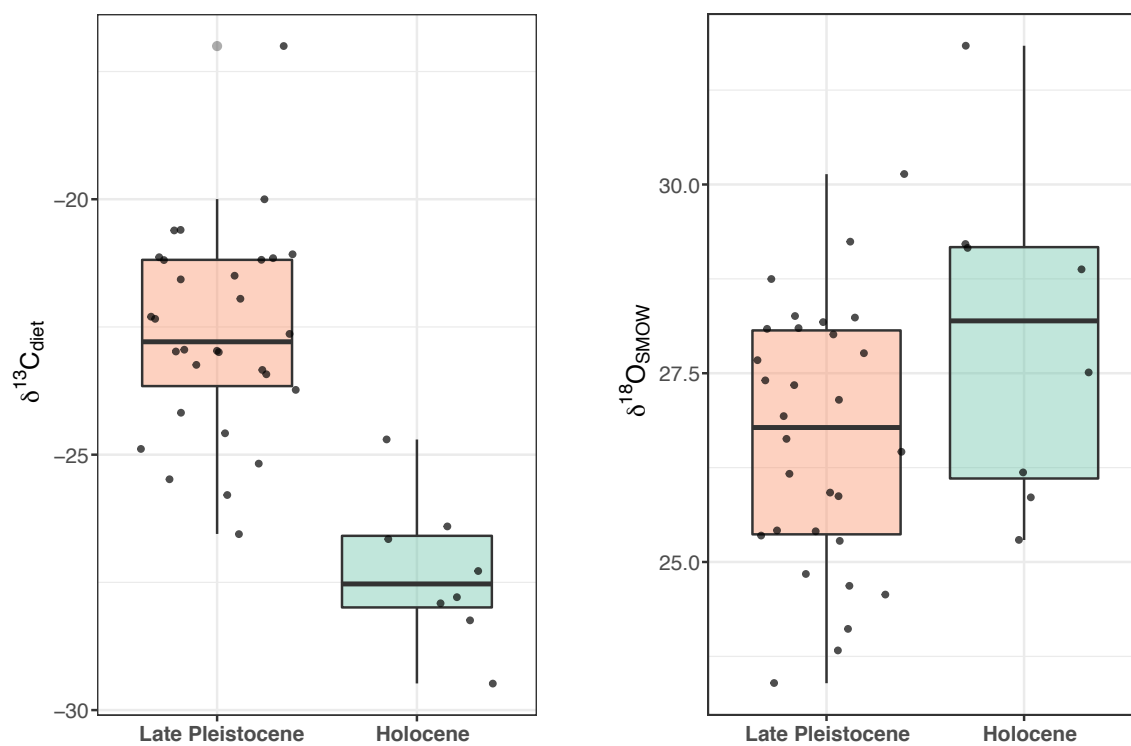
| Specimen ID | Deposit | Excavation Level | Tooth Element | $\delta^{13}\text{C}_{\text{PDB}}$ (‰) | $\delta^{18}\text{O}_{\text{PDB}}$ (‰) |
|-------------|---------|------------------|---------------|--|--|
| ABP 14 | SCCUT | 1 | RM1 | -16.80 | -4.90 |
| ABP 18 | SCCUT | 1 | Lm2 | -13.94 | -4.58 |
| ABP 2 | SCCUT | 1 | Lm2 | -14.57 | -3.30 |
| ABP 22 | SCCUT | 1 | Rm2 | -11.97 | -5.45 |
| ABP 24 | SCCUT | 1 | RM1 | -15.21 | 0.90 |
| ABP 25 | SCCUT | 1 | Rm2 | -15.09 | -1.65 |
| ABP 31 | SCCUT | 1 | RM1 | -13.69 | -1.97 |
| BJZ 1 | SCCUT | 1 | RM1 | -15.55 | -1.70 |
| ABP 38 | SCCUT | 2 | RM1 | -10.68 | -4.84 |
| ABP 46 | SCCUT | 2 | RM1 | -9.88 | -6.04 |
| ABP 50 | SCCUT | 2 | Lm2 | -10.49 | -2.81 |
| ABP 52 | SCCUT | 2 | Lm2 | -8.41 | -6.15 |
| ABP 53 | SCCUT | 2 | RM1 | -10.99 | -4.32 |
| ABP 56 | SCCUT | 3 | RM1 | -11.85 | -3.46 |
| ABP 62 | SCCUT | 3 | RM1 | -8.80 | -4.15 |
| BJZ 20 | SCCUT | 3 | RM1 | -10.21 | -5.89 |
| BJZ 5 | SCCUT | 3 | RM1 | -8.36 | -4.89 |
| DAF 226 | SCCUT | 3 | RM1 | -4.18 | -5.39 |
| MJS 199 | SCCUT | 3 | RM1 | -8.30 | -5.46 |
| MJS 204 | SCCUT | 3 | RM1 | -7.83 | -3.65 |
| MJS 222 | SCCUT | 4 | RM1 | -9.18 | -3.40 |
| MJS 59 | SCCUT | 4 | RM1 | -7.21 | -6.59 |
| MJS 60 | SCCUT | 4 | RM1 | -12.76 | -2.65 |
| MJS 77 | SCCUT | 5 | RM1 | -9.54 | -3.05 |
| ABP 78 | SCCUT | 6 | RM1 | -12.16 | -1.62 |
| MJS 100 | SCCUT | 8 | RM1 | -13.07 | -0.75 |
| MJS 107 | SCCUT | 8 | RM1 | -10.19 | -2.73 |
| MJS 66 | SCCUT | 8 | RM1 | -10.24 | -2.57 |
| BJZ 10a | SCCUT | 9 | RM1 | -11.44 | -2.74 |
| MJS 110 | SCCUT | 9 | Lm2 | -8.42 | -5.34 |
| MJS 113 | SCCUT | 9 | RM1 | -10.59 | -2.10 |
| MJS 117 | SCCUT | 9 | Lm2 | -8.38 | -3.14 |
| MJS 119 | SCCUT | 9 | Lm2 | -12.45 | -3.86 |
| DAF 525 | SCCUT | 10 | Rm2 | -8.73 | -4.60 |
| MJS 120 | SCCUT | 10 | RM1 | -10.23 | -6.87 |
| MJS 122 | SCCUT | 10 | Rm2 | -9.58 | -5.33 |
| MJS 126 | SCCUT | 10 | Lm2 | -7.82 | -7.29 |
| MJS 136 | SCCUT | 10 | RM1 | -13.84 | -2.59 |

Supplemental Table 4 continued.

| Specimen ID | Deposit | Excavation Level | Tooth Element | $\delta^{13}\text{C}_{\text{PDB}}$ (‰) | $\delta^{18}\text{O}_{\text{PDB}}$ (‰) |
|-------------|---------|------------------|---------------|--|--|
| JLB 565 | SCPD | e1 | RM1 | -16.42 | -4.05 |
| JLB 775 | SCPD | e3a | RM1 | -13.41 | -3.91 |
| JLB 776 | SCPD | e3a | RM1 | -10.59 | -3.68 |
| JLB 777 | SCPD | e3a | RM1 | -11.49 | -4.70 |
| JLB 778 | SCPD | e3a | RM1 | -10.61 | -6.19 |
| JLB 771 | SCPD | e3b | RM1 | -7.34 | -5.65 |
| JLB 842 | SCPD | e4a | RM1 | -13.92 | -2.67 |
| JLB 843 | SCPD | e4a | RM1 | -13.67 | -6.83 |
| JLB 844 | SCPD | e4a | RM1 | -5.75 | -6.43 |
| JLB 834 | SCPD | e4b | RM1 | -10.12 | -4.97 |
| JLB 835 | SCPD | e4b | RM1 | -11.63 | -3.90 |
| JLB 837 | SCPD | e4b | RM1 | -14.34 | -3.67 |
| JLB 812 | SCPD | e5a | RM1 | -7.76 | -6.12 |
| JLB 813 | SCPD | e5a | RM1 | -11.28 | -7.00 |
| JLB 815 | SCPD | e5b | RM1 | -14.97 | -5.23 |
| JLB 816 | SCPD | e5b | RM1 | -12.24 | -5.88 |
| JLB 632 | SCPD | e6a | RM1 | -9.68 | -4.02 |
| JLB 747 | SCPD | e7a | RM1 | -5.40 | -3.98 |
| JLB 726 | SCPD | e7b | RM1 | -9.85 | -3.48 |
| JLB 727 | SCPD | e7b | RM1 | -8.97 | -5.79 |
| JLB 728 | SCPD | e7b | RM1 | -9.98 | -4.59 |
| JLB 940 | SCPD | e7b | RM1 | -13.48 | -8.80 |
| JLB 945 | SCPD | e7b | RM1 | -11.59 | -6.27 |
| JLB 657 | SCPD | e8a | RM1 | -11.52 | -7.59 |
| JLB 664 | SCPD | e8a | RM1 | -10.53 | -5.64 |
| JLB 701 | SCPD | e8b | RM1 | -10.91 | -6.90 |
| JLB 706 | SCPD | e8b | RM1 | -10.70 | -5.97 |
| JLB 713 | SCPD | e8b | RM1 | -10.47 | -8.42 |



Supplemental Figure 1: The age model for each level of the SCCUT deposit created using OxCal v4.4.4 (Bronk Ramsey, 2001). Shown are the calibrated radiocarbon age distribution for each sample with the median value indicated, as well as the modelled distribution for the bottom and top boundaries of each phase, with the median boundary age indicated with a †.



Supplemental Figure 2: Boxplot of SCCUT carbon ($\delta^{13}\text{C}$) and oxygen ($\delta^{18}\text{O}$) isotope data for the Late Pleistocene and Holocene groups.

LITERATURE CITED

- Andrews, P. (1990). *Owls, Caves and Fossils. Predation, Preservation and Accumulation of Small Mammal Bones in Caves, with an Analysis of the Pleistocene Cave Faunas From Westbury-Sub-Mendip, Somerset, U.K.* University of Chicago Press.
- Avenant, N. L. (2006). Barn owl pellets: A useful tool for monitoring small mammal communities? *Belgian Journal of Zoology*, 135, 39–43.
- Baker, A., Hartmann, A., Duan, W., Hankin, S., Comas-Bru, L., Cuthbert, M. O., Treble, P. C., Banner, J., Genty, D., Baldini, L. M., Bartolomé, M., Moreno, A., Pérez-Mejías, C., & Werner, M. (2019). Global analysis reveals climatic controls on the oxygen isotope composition of cave drip water. *Nature Communications*, 10(1), 2984. <https://doi.org/10.1038/s41467-019-11027-w>
- Barnosky, A. D., Hadly, E. A., Bascompte, J., Berlow, E. L., Brown, J. H., Fortelius, M., Getz, W. M., Harte, J., Hastings, A., Marquet, P. A., Martinez, N. D., Mooers, A., Roopnarine, P., Vermeij, G., Williams, J. W., Gillespie, R., Kitzes, J., Marshall, C., Matzke, N., ... Smith, A. B. (2012). Approaching a state shift in Earth's biosphere. *Nature*, 486(7401), 52–58. <https://doi.org/10.1038/nature11018>
- Barnosky, A. D., Koch, P. L., Feranec, R. S., Wing, S. L., & Shabel, A. B. (2004). Assessing the Causes of Late Pleistocene Extinctions on the Continents. *Science*, 306(5693), 70–75. <https://doi.org/10.1126/science.1101476>
- Barnosky, A. D., Matzke, N., Tomiya, S., Wogan, G. O. U., Swartz, B., Quental, T. B., Marshall, C., McGuire, J. L., Lindsey, E. L., Maguire, K. C., Mersey, B., & Ferrer, E. A. (2011). Has the Earth's sixth mass extinction already arrived? *Nature*, 471(7336), 51–57. <https://doi.org/10.1038/nature09678>
- Behrensmeyer, A. K., Kidwell, S. M., & Gastaldo, R. A. (2000). Taphonomy and paleobiology. *Paleobiology*, 26(S4), 103–147. <https://doi.org/10.1017/S0094837300026907>
- Bellard, C., Bertelsmeier, C., Leadley, P., Thuiller, W., & Courchamp, F. (2012). Impacts of climate change on the future of biodiversity: Biodiversity and climate change. *Ecology Letters*, 15(4), 365–377. <https://doi.org/10.1111/j.1461-0248.2011.01736.x>
- Birks, H. H., & Birks, H. J. B. (2006). Multi-proxy studies in palaeolimnology. *Vegetation History and Archaeobotany*, 15(4), 235–251. <https://doi.org/10.1007/s00334-006-0066-6>
- Blois, J. L., McGuire, J. L., & Hadly, E. A. (2010). Small mammal diversity loss in response to late-Pleistocene climatic change. *Nature*, 465(7299), 771–774. <https://doi.org/10.1038/nature09077>
- Bronk Ramsey, C. (2001). Development of the Radiocarbon Calibration Program. *Radiocarbon*, 43(2A), 355–363. <https://doi.org/10.1017/S0033822200038212>
- Burbrink, F. T., Chan, Y. L., Myers, E. A., Ruane, S., Smith, B. T., & Hickerson, M. J. (2016). Asynchronous demographic responses to Pleistocene climate change in Eastern Nearctic vertebrates. *Ecology Letters*, 19(12), 1457–1467. <https://doi.org/10.1111/ele.12695>
- Caemmerer, S. von, Ghannoum, O., Pengelly, J. J. L., & Cousins, A. B. (2014). Carbon isotope discrimination as a tool to explore C4 photosynthesis. *Journal of Experimental Botany*, 65(13), 3459–3470. <https://doi.org/10.1093/jxb/eru127>
- California Department of Fish and Game. (2003). *Atlas of the Biodiversity of California*.
- Carraway, L. N., & Verts, B. J. (1991). *Neotoma fuscipes*. *Mammalian Species*, 386, 1. <https://doi.org/10.2307/3504130>
- Cerling, T. E., Wang, Y., & Quade, J. (1993). Expansion of C4 ecosystems as an indicator of global ecological change in the late Miocene. *Nature*, 361(6410), 344–345. <https://doi.org/10.1038/361344a0>

- Clark, P. U., Dyke, A. S., Shakun, J. D., Carlson, A. E., Clark, J., Wohlfarth, B., Mitrovica, J. X., Hostetler, S. W., & McCabe, A. M. (2009). The Last Glacial Maximum. *Science*, 325(5941), 710–714. <https://doi.org/10.1126/science.1172873>
- Clark, P. U., Shakun, J. D., Baker, P. A., Bartlein, P. J., Brewer, S., Brook, E., Carlson, A. E., Cheng, H., Kaufman, D. S., Liu, Z., Marchitto, T. M., Mix, A. C., Morrill, C., Otto-Bliesner, B. L., Pahnke, K., Russell, J. M., Whitlock, C., Adkins, J. F., Blois, J. L., ... Williams, J. W. (2012). Global climate evolution during the last deglaciation. *Proceedings of the National Academy of Sciences*, 109(19). <https://doi.org/10.1073/pnas.1116619109>
- Clementz, M. T. (2012). New insight from old bones: Stable isotope analysis of fossil mammals. *Journal of Mammalogy*, 93(2), 368–380. <https://doi.org/10.1644/11-MAMM-S-179.1>
- Coplen, T. B., Kendall, C., & Hoppole, J. (1983). Comparison of stable isotope reference samples. *Nature*, 302(5905), 236–238. <https://doi.org/10.1038/302236a0>
- Crowley, T. J. (1983). The geologic record of climatic change. *Reviews of Geophysics*, 21(4), 828. <https://doi.org/10.1029/RG021i004p00828>
- Daniels, M. L., Anderson, S., & Whitlock, C. (2005). Vegetation and fire history since the Late Pleistocene from the Trinity Mountains, northwestern California, USA. *The Holocene*, 15(7), 1062–1071. <https://doi.org/10.1191/0959683605hl878ra>
- Dansgaard, W., Johnsen, S. J., Clausen, H. B., Dahl-Jensen, D., Gundestrup, N. S., Hammer, C. U., Hvidberg, C. S., Steffensen, J. P., Sveinbjörnsdóttir, A. E., Jouzel, J., & Bond, G. (1993). Evidence for general instability of past climate from a 250-kyr ice-core record. *Nature*, 364(6434), 218–220. <https://doi.org/10.1038/364218a0>
- Davidson, T. A., Reid, M. A., Sayer, C. D., & Chilcott, S. (2013). Palaeolimnological records of shallow lake biodiversity change: Exploring the merits of single versus multi-proxy approaches. *Journal of Paleolimnology*, 49(3), 431–446. <https://doi.org/10.1007/s10933-013-9696-8>
- Delaygue, G. (2009). Oxygen Isotopes. In V. Gornitz (Ed.), *Encyclopedia of Paleoclimatology and Ancient Environments* (pp. 666–673). Springer Netherlands. https://doi.org/10.1007/978-1-4020-4411-3_163
- Eberle, J. J., Fricke, H. C., Humphrey, J. D., Hackett, L., Newbrey, M. G., & Hutchison, J. H. (2010). Seasonal variability in Arctic temperatures during early Eocene time. *Earth and Planetary Science Letters*, 296(3–4), 481–486. <https://doi.org/10.1016/j.epsl.2010.06.005>
- Ehleringer, J. R., & Cooper, T. A. (1988). Correlations between carbon isotope ratio and microhabitat in desert plants. *Oecologia*, 76(4), 562–566. <https://doi.org/10.1007/BF00397870>
- FAUNMAP Working Group. 1994. FAUNMAP: a database documenting late Quaternary distributions of mammal species in the United States. *Illinois State Museum Scientific Papers* 25(1-2):1-690. (n.d.).
- Feranec, R. S., Hadly, E. A., & Paytan, A. (2010). Isotopes reveal limited effects of middle Pleistocene climate change on the ecology of mid-sized mammals. *Quaternary International*, 217(1–2), 43–52. <https://doi.org/10.1016/j.quaint.2009.07.018>
- Fernández-García, M., Royer, A., López-García, J. M., Bennàsar, M., Goedert, J., Fourel, F., Julien, M.-A., Bañuls-Cardona, S., Rodríguez-Hidalgo, A., Vallverdú, J., & Lécuyer, C. (2019). Unravelling the oxygen isotope signal ($\delta^{18}\text{O}$) of rodent teeth from northeastern Iberia, and implications for past climate reconstructions. *Quaternary Science Reviews*, 218, 107–121. <https://doi.org/10.1016/j.quascirev.2019.04.035>
- Fox, N. (n.d.). Millennial-Scale Drivers of Small Mammal Isotopic Niche Dynamics in Southern California. https://papers.ssrn.com/sol3/papers.cfm?abstract_id=4119786
- Gehler, A., Tütken, T., & Pack, A. (2012). Oxygen and Carbon Isotope Variations in a Modern Rodent Community – Implications for Palaeoenvironmental Reconstructions. *PLoS ONE*, 7(11), e49531. <https://doi.org/10.1371/journal.pone.0049531>

- Gill, J. L., Williams, J. W., Jackson, S. T., Lininger, K. B., & Robinson, G. S. (2009). Pleistocene Megafaunal Collapse, Novel Plant Communities, and Enhanced Fire Regimes in North America. *Science*, 326(5956), 1100–1103. <https://doi.org/10.1126/science.1179504>
- Graham, R. W., Lundelius, E. L., Graham, M. A., Schroeder, E. K., Toomey, R. S., Anderson, E., Barnosky, A. D., Burns, J. A., Churcher, C. S., Grayson, D. K., Guthrie, R. D., Harington, C. R., Jefferson, G. T., Martin, L. D., McDonald, H. G., Morlan, R. E., Semken, H. A., Webb, S. D., Werdelin, L., & Wilson, M. C. (1996). Spatial Response of Mammals to Late Quaternary Environmental Fluctuations. *Science*, 272(5268), 1601–1606. <https://doi.org/10.1126/science.272.5268.1601>
- Grimes, S. T., Matthey, David. P., Collinson, M. E., & Hooker, J. J. (2004). Using mammal tooth phosphate with freshwater carbonate and phosphate palaeoproxies to obtain mean paleotemperatures. *Quaternary Science Reviews*, 23(7–8), 967–976. <https://doi.org/10.1016/j.quascirev.2003.06.023>
- Haslett, J., & Parnell, A. (2008). A simple monotone process with application to radiocarbon-dated depth chronologies. *Journal of the Royal Statistical Society: Series C (Applied Statistics)*, 57(4), 399–418. <https://doi.org/10.1111/j.1467-9876.2008.00623.x>
- Heaton, T. H. E. (1999). Spatial, Species, and Temporal Variations in the $^{13}\text{C}/^{12}\text{C}$ Ratios of C3 Plants: Implications for Palaeodiet Studies. *Journal of Archaeological Science*, 26(6), 637–649. <https://doi.org/10.1006/jasc.1998.0381>
- Hedges, R. E. M., & Reynard, L. M. (2007). Nitrogen isotopes and the trophic level of humans in archaeology. *Journal of Archaeological Science*, 34(8), 1240–1251. <https://doi.org/10.1016/j.jas.2006.10.015>
- Jeffrey, A., Denys, C., Stoetzel, E., & Lee-Thorp, J. A. (2015). Influences on the stable oxygen and carbon isotopes in gerbillid rodent teeth in semi-arid and arid environments: Implications for past climate and environmental reconstruction. *Earth and Planetary Science Letters*, 428, 84–96. <https://doi.org/10.1016/j.epsl.2015.07.012>
- Jones, D. B., & Desantis, L. R. G. (2017). Dietary ecology of ungulates from the La Brea tar pits in southern California: A multi-proxy approach. *Palaeogeography, Palaeoclimatology, Palaeoecology*, 466, 110–127. <https://doi.org/10.1016/j.palaeo.2016.11.019>
- Kelly, J. F. (2000). Stable isotopes of carbon and nitrogen in the study of avian and mammalian trophic ecology. *Canadian Journal of Zoology*, 78(1), 1–27. <https://doi.org/10.1139/z99-165>
- Koch, P. L. (1998). Isotopic reconstruction of past continental environments. *Annual Review of Earth and Planetary Sciences*, 26(1), 573–613. <https://doi.org/10.1146/annurev.earth.26.1.573>
- Koch, P. L., Tuross, N., & Fogel, M. L. (1997). The Effects of Sample Treatment and Diagenesis on the Isotopic Integrity of Carbonate in Biogenic Hydroxylapatite. *Journal of Archaeological Science*, 24, 417–429.
- Kohn, M. J. (2010). Carbon isotope compositions of terrestrial C3 plants as indicators of (paleo)ecology and (paleo)climate. *Proceedings of the National Academy of Sciences*, 107(46), 19691–19695. <https://doi.org/10.1073/pnas.1004933107>
- Kohn, M. J., & McKay, M. P. (2012). Paleoeology of late Pleistocene–Holocene faunas of eastern and central Wyoming, USA, with implications for LGM climate models. *Palaeogeography, Palaeoclimatology, Palaeoecology*, 326–328, 42–53. <https://doi.org/10.1016/j.palaeo.2012.01.037>
- Lee-Thorp, J. A., Sealy, J. C., & van der Merwe, N. J. (1989). Stable carbon isotope ratio differences between bone collagen and bone apatite, and their relationship to diet. *Journal of Archaeological Science*, 16(6), 585–599. [https://doi.org/10.1016/0305-4403\(89\)90024-1](https://doi.org/10.1016/0305-4403(89)90024-1)
- Matias, M. G., Pereira, C. L., Raposeiro, P. M., Gonçalves, V., Cruz, A. M., Costa, A. C., & Araújo, M. B. (2017). Divergent trophic responses to biogeographic and environmental gradients. *Oikos*, 126(1), 101–110. <https://doi.org/10.1111/oik.02604>
- McElwain, J. C., & Punyasena, S. W. (2007). Mass extinction events and the plant fossil record. *Trends in Ecology & Evolution*, 22(10), 548–557. <https://doi.org/10.1016/j.tree.2007.09.003>

- McLean, B. S., & Emslie, S. D. (2012). Stable isotopes reflect the ecological stability of two high-elevation mammals from the late Quaternary of Colorado. *Quaternary Research*, 77(3), 408–417. <https://doi.org/10.1016/j.yqres.2012.02.001>
- Mohr, J. A., Whitlock, C., & Skinner, C. N. (2000). Postglacial vegetation and fire history, eastern Klamath Mountains, California, USA. *The Holocene*, 10(5), 587–601. <https://doi.org/10.1191/095968300675837671>
- North Greenland Ice Core Project members. (2004). High-resolution record of Northern Hemisphere climate extending into the last interglacial period. *Nature*, 431(7005), 147–151. <https://doi.org/10.1038/nature02805>
- O’Leary, M. H. (1988). Carbon Isotopes in Photosynthesis. *BioScience*, 38(5), 328–336. <https://doi.org/10.2307/1310735>
- Oster, J. L., Montañez, I. P., Sharp, W. D., & Cooper, K. M. (2009). Late Pleistocene California droughts during deglaciation and Arctic warming. *Earth and Planetary Science Letters*, 288(3–4), 434–443. <https://doi.org/10.1016/j.epsl.2009.10.003>
- Oster, J. L., Weisman, I. E., & Sharp, W. D. (2020). Multi-proxy stalagmite records from northern California reveal dynamic patterns of regional hydroclimate over the last glacial cycle. *Quaternary Science Reviews*, 241, 106411. <https://doi.org/10.1016/j.quascirev.2020.106411>
- Passey, B. H., Robinson, T. F., Ayliffe, L. K., Cerling, T. E., Sponheimer, M., Dearing, M. D., Roeder, B. L., & Ehleringer, J. R. (2005). Carbon isotope fractionation between diet, breath CO₂, and bioapatite in different mammals. *Journal of Archaeological Science*, 32(10), 1459–1470. <https://doi.org/10.1016/j.jas.2005.03.015>
- Pedro, J. B., Rasmussen, S. O., & van Ommen, T. D. (2012). Tightened constraints on the time-lag between Antarctic temperature and CO₂ during the last deglaciation. *Climate of the Past*, 8(4), 1213–1221. <https://doi.org/10.5194/cp-8-1213-2012>
- Peneycad, E., Candy, I., & Schreve, D. C. (2019). Variability in the oxygen isotope compositions of modern rodent tooth carbonate: Implications for palaeoclimate reconstructions. *Palaeogeography, Palaeoclimatology, Palaeoecology*, 514, 695–705. <https://doi.org/10.1016/j.palaeo.2018.11.017>
- Pisias, N. G., & Moore, T. C. (1981). The evolution of Pleistocene climate: A time series approach. *Earth and Planetary Science Letters*, 52(2), 450–458. [https://doi.org/10.1016/0012-821X\(81\)90197-7](https://doi.org/10.1016/0012-821X(81)90197-7)
- Platt, D. E., Haber, M., Dagher-Kharrat, M. B., Douaihy, B., Khazen, G., Ashrafian Bonab, M., Salloum, A., Mouzaya, F., Luiselli, D., Tyler-Smith, C., Renfrew, C., Matisoo-Smith, E., & Zalloua, P. A. (2017). Mapping Post-Glacial expansions: The Peopling of Southwest Asia. *Scientific Reports*, 7(1), 40338. <https://doi.org/10.1038/srep40338>
- Podlesak, D. W., Torregrossa, A.-M., Ehleringer, J. R., Dearing, M. D., Passey, B. H., & Cerling, T. E. (2008). Turnover of oxygen and hydrogen isotopes in the body water, CO₂, hair, and enamel of a small mammal. *Geochimica et Cosmochimica Acta*, 72(1), 19–35. <https://doi.org/10.1016/j.gca.2007.10.003>
- Porder, S., Paytan, A., & Hadly, E. A. (2003). Mapping the origin of faunal assemblages using strontium isotopes. *Paleobiology*, 29(2), 197–204. [https://doi.org/10.1666/0094-8373\(2003\)029<0197:MTOOFA>2.0.CO;2](https://doi.org/10.1666/0094-8373(2003)029<0197:MTOOFA>2.0.CO;2)
- Quintero, I., & Wiens, J. J. (2013). Rates of projected climate change dramatically exceed past rates of climatic niche evolution among vertebrate species. *Ecology Letters*, 16(8), 1095–1103. <https://doi.org/10.1111/ele.12144>
- R: A language and environment for statistical computing. (2020). R Foundation for Statistical Computing, Vienna, Austria. <https://www.R-project.org/>
- Reimer, P. J., Austin, W. E. N., Bard, E., Bayliss, A., Blackwell, P. G., Bronk Ramsey, C., Butzin, M., Cheng, H., Edwards, R. L., Friedrich, M., Grootes, P. M., Guilderson, T. P., Hajdas, I., Heaton, T. J., Hogg, A. G., Hughen, K. A., Kromer, B., Manning, S. W., Muscheler, R., ...

- Talamo, S. (2020). The IntCal20 Northern Hemisphere Radiocarbon Age Calibration Curve (0–55 cal kBP). *Radiocarbon*, 62(4), 725–757. <https://doi.org/10.1017/RDC.2020.41>
- Reimer, Paula J., Baillie, Mike G. L., Bard, Edouard, Bayliss, Alex, Beck, J. Warren, Bertrand, Chanda J. H., Blackwell, Paul G., Buck, Caitlin E., Burr, George S., Cutler, Kirsten B., Damon, Paul E., Edwards, R. Lawrence, Fairbanks, Richard G., Friedrich, Michael, Guilderson, Thomas P., Hogg, Alan G., Hughen, Konrad A., Kromer, Bernd, McCormac, Gerry, ... Weyhenmeyer, Constanze E. (2004). Intcal04 Terrestrial Radiocarbon Age Calibration, 0–26 Cal Kyr BP. *Radiocarbon*, 46(3), 1029–1058. <https://doi.org/10.1017/S0033822200032999>
- Royer, A., Lécuyer, C., Montuire, S., Amiot, R., Legendre, S., Cuenca-Bescós, G., Jeannet, M., & Martineau, F. (2013). What does the oxygen isotope composition of rodent teeth record? *Earth and Planetary Science Letters*, 361, 258–271. <https://doi.org/10.1016/j.epsl.2012.09.058>
- Scott Anderson, R., Smith, S. J., Jass, R. B., & Geoffrey Spaulding, W. (2008). A Late Holocene Record of Vegetation and Climate from a Small Wetland in Shasta County, California. *Madroño*, 55(1), 15–25. [https://doi.org/10.3120/0024-9637\(2008\)55\[15:ALHROV\]2.0.CO;2](https://doi.org/10.3120/0024-9637(2008)55[15:ALHROV]2.0.CO;2)
- Simms, M. J. (1994). Emplacement and preservation of vertebrates in caves and fissures. *Zoological Journal of the Linnean Society*, 112(1–2), 261–283. <https://doi.org/10.1111/j.1096-3642.1994.tb00320.x>
- Sponheimer, M., & Lee-Thorp, J. A. (1999). Oxygen Isotopes in Enamel Carbonate and their Ecological Significance. *Journal of Archaeological Science*, 26(6), 723–728. <https://doi.org/10.1006/jasc.1998.0388>
- Steffensen, J. P., Andersen, K. K., Bigler, M., Clausen, H. B., Dahl-Jensen, D., Fischer, H., Goto-Azuma, K., Hansson, M., Johnsen, S. J., Jouzel, J., Masson-Delmotte, V., Popp, T., Rasmussen, S. O., Röthlisberger, R., Ruth, U., Stauffer, B., Siggaard-Andersen, M.-L., Sveinbjörnsdóttir, Á. E., Svensson, A., & White, J. W. C. (2008). High-Resolution Greenland Ice Core Data Show Abrupt Climate Change Happens in Few Years. *Science*, 321(5889), 680–684. <https://doi.org/10.1126/science.1157707>
- Stralberg, D., Jongsomjit, D., Howell, C. A., Snyder, M. A., Alexander, J. D., Wiens, J. A., & Root, T. L. (2009). Re-Shuffling of Species with Climate Disruption: A No-Analog Future for California Birds? *PLoS ONE*, 4(9), e6825. <https://doi.org/10.1371/journal.pone.0006825>
- Terry, R. C. (2018). Isotopic niche variation from the Holocene to today reveals minimal partitioning and individualistic dynamics among four sympatric desert mice. *Journal of Animal Ecology*, 87(1), 173–186. <https://doi.org/10.1111/1365-2656.12771>
- Tomé, C. P., Lyons, S. K., Newsome, S. D., & Smith, F. A. (2021). The sensitivity of *Neotoma* to climate change and biodiversity loss over the late Quaternary. *Quaternary Research*, 105, 49–63. <https://doi.org/10.1017/qua.2021.29>
- Tomé, C. P., Lyons, S. K., Newsome, S. D., & Smith, F. A. (2022). The sensitivity of *Neotoma* to climate change and biodiversity loss over the late Quaternary. *Quaternary Research*, 105, 49–63. <https://doi.org/10.1017/qua.2021.29>
- Tooth, A. F., & Fairchild, I. J. (2003). Soil and karst aquifer hydrological controls on the geochemical evolution of speleothem-forming drip waters, Crag Cave, southwest Ireland. *Journal of Hydrology*, 273(1–4), 51–68. [https://doi.org/10.1016/S0022-1694\(02\)00349-9](https://doi.org/10.1016/S0022-1694(02)00349-9)
- Tremaine, D. M., & Froelich, P. N. (2013). Speleothem trace element signatures: A hydrologic geochemical study of modern cave dripwaters and farmed calcite. *Geochimica et Cosmochimica Acta*, 121, 522–545. <https://doi.org/10.1016/j.gca.2013.07.026>
- Twitchett, R. J. (2006). The palaeoclimatology, palaeoecology and palaeoenvironmental analysis of mass extinction events. *Palaeogeography, Palaeoclimatology, Palaeoecology*, 232(2–4), 190–213. <https://doi.org/10.1016/j.palaeo.2005.05.019>
- van der Merwe, N. J., & Medina, E. (1991). The canopy effect, carbon isotope ratios and foodwebs in amazonia. *Journal of Archaeological Science*, 18(3), 249–259. [https://doi.org/10.1016/0305-4403\(91\)90064-V](https://doi.org/10.1016/0305-4403(91)90064-V)

- Whitlock, C., & Bartlein, P. J. (1997). Vegetation and climate change in northwest America during the past 125 kyr. *Nature*, 388(6637), 57–61. <https://doi.org/10.1038/40380>
- Williams, J. W., Shuman, B. N., Webb, T., Bartlein, P. J., & Leduc, P. L. (2004). LATE-QUATERNARY VEGETATION DYNAMICS IN NORTH AMERICA: SCALING FROM TAXA TO BIOMES. *Ecological Monographs*, 74(2), 309–334. <https://doi.org/10.1890/02-4045>